0 mpp), indicating that the conserved motif found within p22 can substitute for the signal found within G and is therefore a functional ER export signal. In contrast, and similar to G(6xA), G/AXΦA had significantly decreased kinetics of ER export ($p \leq 0.001$ for all time points except 0 mpp). The ability of G/AXΦA to ultimately become resistant to EndoH digestion more efficiently than G(6xA) is likely attributable to the presence of the aspartic acid residue on G/AXΦA, which has previously been shown to improve ER export efficiency compared to alanines alone [9,10,40]. In addition, the Golgi was phenotypically intact in cells expressing both wildtype G and G/p22 (data not shown), suggesting that protein trafficking is not inhibited due solely to the presence of the YXΦESDG motif.

Taken together, these data suggest that the motif found within p22 can function for the well-characterized ER export signal found within VSV G and thus this motif constitutes a true ER export signal. For this reason, we henceforth refer to the YXΦESDG motif within p22 as a mimic of an ER export signal, or MERES, motif. In addition, mutation of two residues within the MERES motif that are critical to the function of p22 is sufficient to decrease ER export efficiency. This observation coupled with the inability of the MERES motif alone to induce Golgi disassembly when expressed on VSV G demonstrated that it alone is insufficient to antagonize ER/Golgi trafficking.

p22 targets COPII, but not COPI, trafficking

We lastly sought to determine, first, what is the fate of the cargo in the secretory pathway? And second, does p22 target the anterograde or retrograde pathway of ER/Golgi trafficking? To answer both of these questions, we utilized the SEAP vector described above to monitor the localization of COPI and COPII vesicle marker proteins with respect to secretory pathway cargo, in this case again monitoring SEAP itself as the cargo, and alterations that occur due to the presence of p22.

The 3A protein from several picornaviruses inhibits protein secretion by deregulating COPI vesicle budding from the *cis* Golgi [12,13,43]. To determine if p22 might utilize a similar mechanism of action, the phenotype of COPI vesicle transport in cells expressing p22 was explored by immunofluoresence of the COPI marker protein β-COP. In the presence of GFP alone, SEAP was present only in an intact Golgi, where COPI puncta are prominently, though not exclusively, localized (Figure 7A). As expected, SEAP was prominently retained in cells expressing both PV 3A (Figure 7B) and NV p22 (Figure 7C), although with different phenotypic localizations. In 3A-expressing cells, COPI puncta were diffuse and unapparent, and SEAP was retained in diffuse, minimally punctate cellular structures reminiscent of Golgi that has been redistributed into the ER due to antagonism of trafficking by 3A, as has been reported previously [12,34,44]. In contrast, COPI puncta in cells expressing p22 were apparent but re-localized widely throughout the cytoplasm, demonstrating a failure of these vesicles to properly localize and/or traffic within cells. SEAP in p22-positive cells was present both in discrete punctate vesicles that did not co-localize with COPI puncta, and also in peri-Golgi clusters that did co-localize with COPI puncta. This suggested that SEAP, and therefore cellular cargo, was being retained in non-COPI puncta and at a *cis* Golgi site due to the expression of p22. This suggested that the retrograde, Golgi-to-ER arm of the secretory pathway was intact, but an aspect of the forward pathway was non-functional in p22-expressing cells. These data demonstrate that, in contrast to 3A, p22 does not specifically target COPI trafficking, but does induce cellular cargo retention between the ER and Golgi.

Due to these observations and because ER export signals promote the rapid and direct uptake of cargo into COPII-coated vesicles, which are necessary for ER-to-Golgi protein trafficking, we hypothesized that p22 is acting on the forward, ER-to-Golgi trafficking pathway to inhibit COPII vesicle budding or trafficking to the Golgi to thereby induce Golgi disassembly and inhibit protein secretion. To test this hypothesis, we again examined the specific sub-cellular localization of the retained SEAP that was present in discrete cytoplasmic puncta. Under the same di-cistronic SEAP expression system, in the presence of GFP alone SEAP was again localized exclusively in a phenotypically intact Golgi with COPII puncta immediately surrounding it, although with a near complete lack of co-localization with COPII puncta (Figure 8A). In contrast, in the presence of p22 SEAP was localized in peri-nuclear puncta (Figure 8B), similar to the phenotype of a disassembled Golgi previously described (Figure 2A). Both SEAP and p22 also co-localized with COPII puncta that were also prominently re-localized to the same presumably peri-Golgi structures, although there was some diffuse, likely ER-localized, COPII staining that did not localize with either p22 or SEAP. Additionally, these discrete p22-positive puncta co-localized with SEAP and COPII vesicles (Figure 8B, inset). This suggested that p22 and SEAP are retained with COPII puncta that have properly budded from the ER, but have been mislocalized and did not properly traffic into the Golgi. Due to the apparent size of the p22/SEAP/COPII puncta observed by immuno-fluorescence, it is tempting to speculate that the cellular vesicles with cargo inside them that were observed by EM (Figure 3B) may be enlarged COPII puncta that were mislocalized within cells. When the AXΦA mutant of p22 was expressed, SEAP and COPII puncta both returned to a wild type distribution (Figure 8C) that was phenotypically indistinguishable from cells expressing GFP alone. This demonstrated that, in the presence of p22 and dependent upon the MERES motif, both COPII puncta and their cargo are mislocalized, suggestive of a failure of vesicles to either traffic to or fuse with the Golgi apparatus.

Discussion

We have described for the first time a novel function for the Norwalk virus nonstructural protein p22. The major new findings of this study can be summarized as follows: 1) independent expression of p22 disassembles the Golgi, which also occurs during NV replication, and inhibits cellular protein secretion; 2) subcellular localization of p22 depends on a motif that mimics a cellular ER export signal in both sequence and function, which we have named a MERES motif; and 3) p22 depends on the MERES motif likely to antagonize COPII vesicle trafficking, resulting in Golgi disassembly and an inhibition of cellular protein secretion. Due to the observed trafficking of p22, we propose that p22 is initially localized to the membranes of the secretory pathway via amino acids 103–148, which contain a membrane association domain. The MERES motif then mediates the uptake of p22 onto COPII vesicles, which mislocalize within cells and inhibit, by an as-of-yet undetermined mechanism, proper trafficking to or fusion with the Golgi. Restricting the proper flow of COPII vesicles then induces disassembly of the Golgi and ultimately results in an inhibition of cellular protein secretion.

The MERES motif found within p22 is somewhat unconventional for an ER export signal in that p22 does not encode a signal sequence to mediate ER import, is not glycosylated, and is not exclusively ER localized at any point during expression (Figure 4D and data not shown). Moreover, it has several unique features compared to other known di-acidic ER export signals. First,

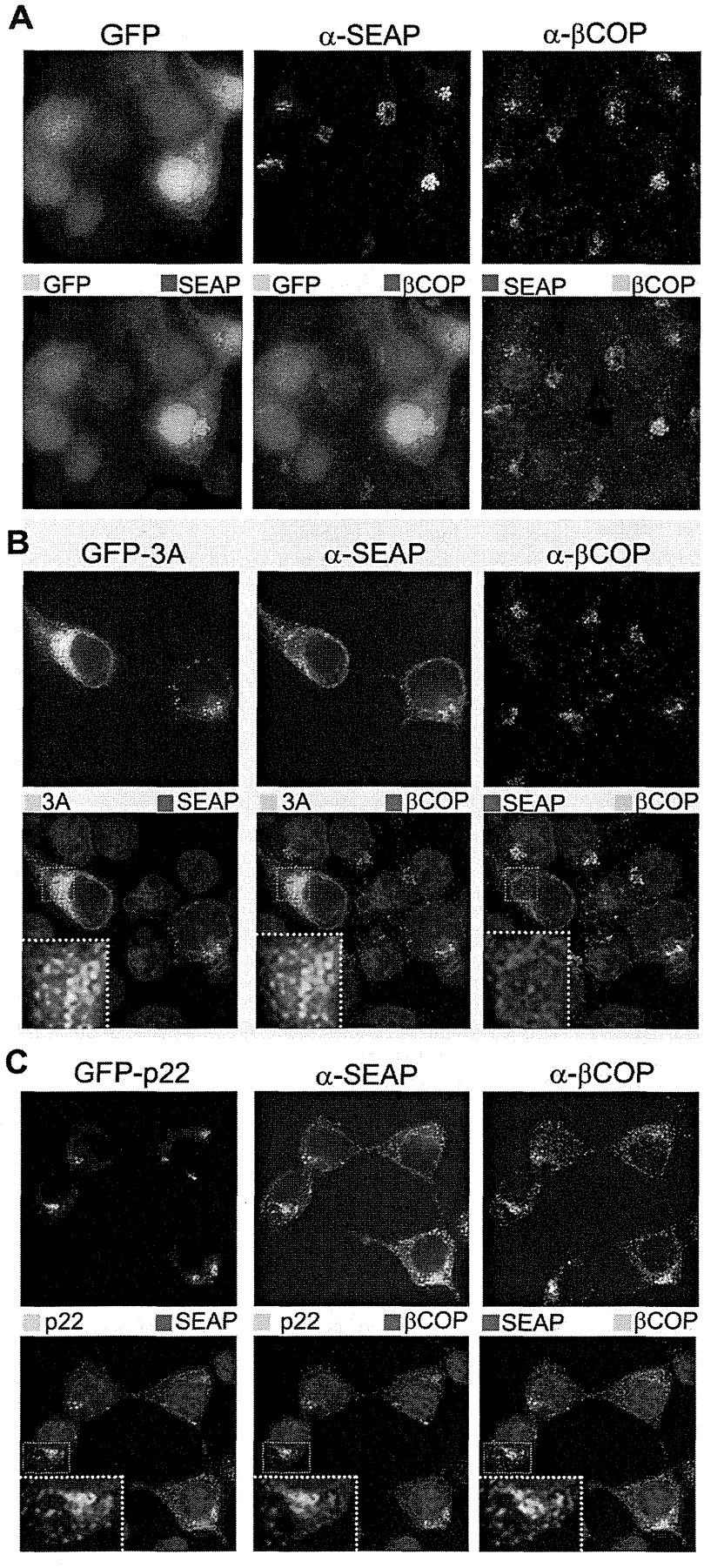
A
GFP
α-SEAP
α-βCOP
GFP
SEAP
GFP
βCOP
SEAP
βCOP
B
GFP-3A
α-SEAP
α-βCOP
3A
SEAP
3A
βCOP
SEAP
βCOP
C
GFP-p22
α-SEAP
α-βCOP
p22
SEAP
p22
βCOP
SEAP
βCOP

Figure 7. SEAP is differentially retained in the presence of PV 3A and NV p22. Cells expressing GFP alone (**A**), or GFP-tagged 3A (**B**) or NV p22 (**C**) were fixed at 24 hpt and immuno-stainined with antibody against SEAP (Alexa 594-conjugated secondary antibody) and the COPI marker protein β-COP (Alexa 647-conjugated secondary antibody), stained with DAPI (blue fluorescence), and imaged by deconvolution microscopy. Channels were pseudo-colored as indicated for merged images. Insets in **B** and **C** represent a 6X zoom of the boxed region.
doi:10.1371/journal.pone.0013130.g007

instead of the tyrosine residue being located between the MAD and the acidic residues, it is located N terminal to the acidic residues and MAD. Second, instead of encoding two amino acids between the Y and Φ residues, p22 encodes only a single residue. Third, most, though not all, ER export signals are located towards the extreme C terminus of proteins, whereas the signal found within p22 is located in the middle of the protein. The human asialoglycoprotein receptor H1 subunit is the only other protein described to have this arrangement of a di-acidic ER export signal [9]. Additionally, we have no data to support any portion of p22 being present inside the lumen of the ER and instead p22 appears to be a peripheral membrane protein based on sodium carbonate extraction (data not shown). For these reasons, the YXΦESDG motif found within p22, though similar in sequence and function to a traditional di-acidic ER export signal, may in reality simply mimic the function of these signals to exploit the cellular machinery responsible for protein secretion in order to recruit p22 to COPII vesicles. This lends support to the nomenclature of this motif being a mimic of an ER export signal, as it shares many of the features and effects of a traditional ER export signal, but ultimately has a unique composition and function.

Furthermore, p22 seems to depend on the MERES motif to function as a secretory pathway inhibitor; however this motif alone is not responsible for antagonism, as replacement of the ER export signal from VSV G with the MERES motif functionally restored ER export efficiency without any obvious impediment. In support of this, none of the deletion mutants of p22 induced Golgi disassembly, although amino acids 50–148 were sufficient to mediate Golgi localization. Similarly, these same residues were sufficient to mediate COPII localization, but do not lead to the mislocalization of COPII puncta (data not shown) that was observed for full length p22. Taken together, these data suggest that the MERES motif of p22 alone is necessary but not sufficient to inhibit the secretory pathway. A second as-of-yet uncharacterized factor, contained within or dependent on the N and/or C termini based on deletion mutant experimentation, is required as a subsequent step in secretory pathway antagonism. This idea is substantiated by chimeric G/p22 properly trafficking to the Golgi and becoming resistant to Endo H digestion with kinetics equivalent to wildtype G. Possibilities for the function of this second factor are many, including binding to and/or disrupting a cellular tethering protein [45,46] or a member of the p24 family that covers COPII vesicles [47], or antagonizing SNARE-mediated vesicle fusion by interaction with a regulatory protein such as VAP-A/B [48], all of which are critical components of ER/Golgi trafficking. This latter possibility is especially attractive, as VAP-B has previously been demonstrated to be a binding partner for another Norwalk virus nonstructural protein [49], and thus may be an over-arching target of the secretory pathway by noroviruses. Both of these possibilities are currently under investigation as potential targets for p22 and as scaffolding factors upon which noroviruses may anchor their genome replication.

The data presented in this study support, but do not prove, that p22 targets COPII vesicle trafficking; this is further complicated by the examination of cells by immunofluorescence primarily at 24 hpt, which may not reflect steady-state localization. Proving this mechanism will require demonstrating a specific binding to or inhibition of the trafficking of COPII vesicles using *in vitro* assays. Unfortunately, these studies have not been possible due to the inability of producing purified p22 for such studies as well as the lack of an antibody to p22 that allows for immunoprecipitation assays. Therefore, until a direct interaction is demonstrated, it remains possible that p22 could target a non-COPII aspect of the secretory pathway to mediate inhibition. p22 does not activate Arf1 or Sar1 (data not shown), making targeting of the formation of COPI vesicles in the same manner as PV and CVB3 3A, or COPII vesicles by a unique approach, unlikely. A *trans* Golgi mechanism of action seems similarly unlikely based on lack of localization of wildtype p22 with the trans Golgi marker protein golgin 97 (Figure S2); the same is also true for possible targeting of endosomes by p22 (data not shown). Thus, although there are many possible alternative explanations for the observed effects of p22, specific targeting and mislocalization of COPII vesicles is at present the most likely explanation.

Although no other cellular or microbial protein to date has been described to use the arrangement of a MERES motif that p22 employs to inhibit the secretory pathway, several previously characterized secretory pathway antagonists have potential ER export signals or mimics thereof. The *Eschericia coli* protein NleA inhibits COPII-dependent export from the ER by direct interaction with Sec24 [50], and the cellular proteins STAM-1 and -2, which are involved in the signaling of growth factors and cytokines, regulate Golgi architecture by interaction the Sec13/31 COPII cage components [51]. Examination of the primary amino acid sequence of NleA and STAM-1/2 revealed motifs similar to a di-acidic ER export signal (unpublished observation). If further studies determine these motifs directly contribute to either the cellular localization or, for STAM-1/2, proper ER export, this would provide support for the idea that ER export signals or their mimics can be used not only to facilitate ER export, but also to promote interaction with COPII vesicles to mediate specific antagonism of the secretory pathway.

Both similarities and differences were noted between p22 and the picornavirus 3A protein. Both proteins localize to membranes via an amphipathic alpha helix, and both inhibit ER-to-Golgi trafficking to decrease cellular protein secretion. However, the mechanism of this shutoff appears to be quite distinct between Norwalk virus and picornaviruses. Inhibition of protein secretion and Golgi disassembly are in some cases separable and distinct, as is the case for PV infection [44], whereas in other cases one will follow the other, for example during cell division [31,52]. There were also clear ultrastructural similarities between cells expressing p22 and 3A in inducing the accumulation of free membranes, double-membrane vesicles and vacuoles [12,34], although cells expressing p22 did not exhibit the swelling of the ER reported for PV 3A [34] or the crystalloid ER patterns seen after expression of the hepatitis A virus 2C and 2BC proteins that also induce significant membrane rearrangements [53]. This further supports the similarity of p22 and 3A in secretory pathway antagonism, but through different arms of this pathway. NV p22 therefore may be more similar in the cellular effects of the hepatitis C virus NS4A/B protein, which, though less studied than PV 3A, antagonizes ER-to-Golgi trafficking, and induces the accumulation of "membranous webs," vacuoles and double-membrane vesicles, but not ER swelling [54].

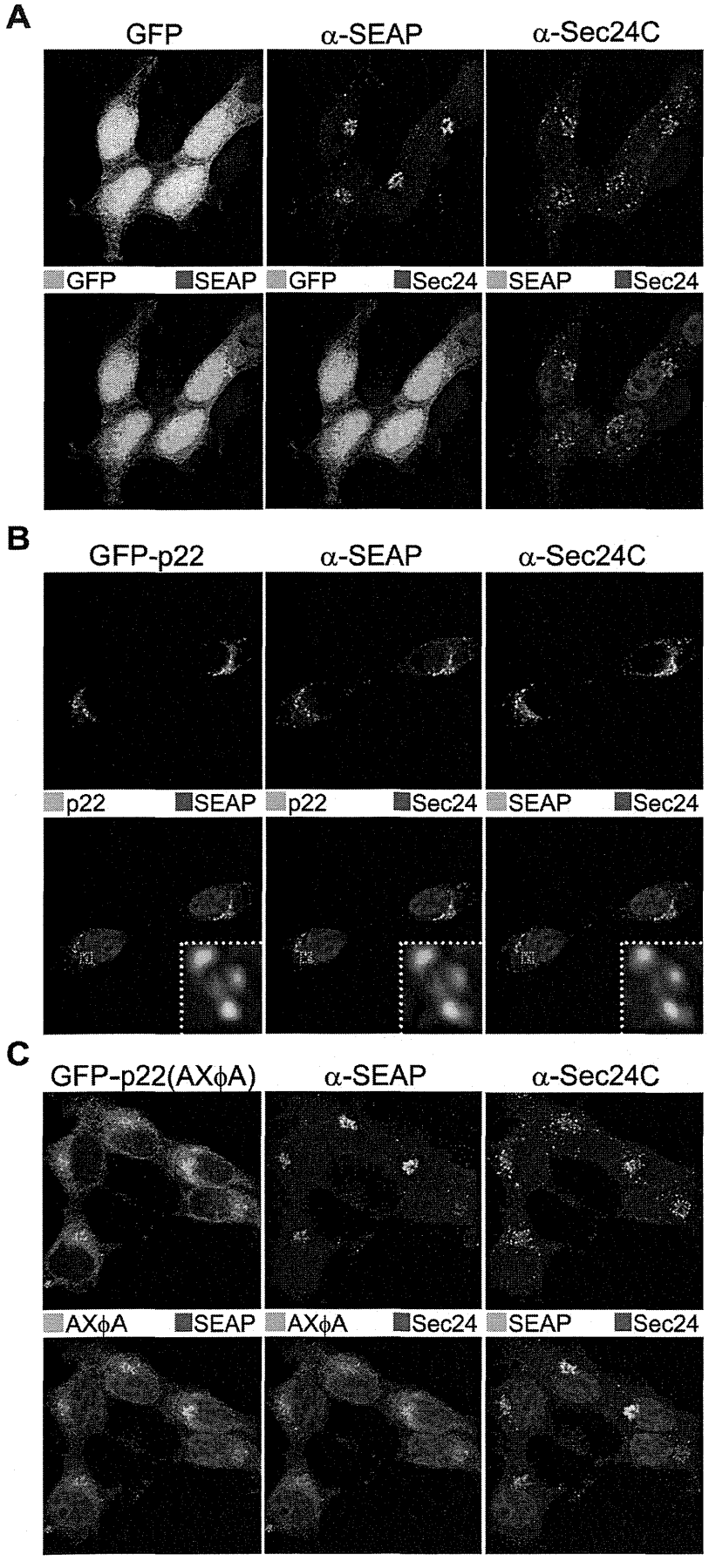
A
GFP
α-SEAP
α-Sec24C
GFP
SEAP
GFP
Sec24
SEAP
Sec24
B
GFP-p22
α-SEAP
α-Sec24C
p22
SEAP
p22
Sec24
SEAP
Sec24
C
GFP-p22(AXϕA)
α-SEAP
α-Sec24C
AXϕA
SEAP
AXϕA
Sec24
SEAP
Sec24

Figure 8. Secretory pathway cargo is retained in COPII vesicles in the presence of p22, but not p22(AXΦA). Cells expressing GFP alone (**A**), or GFP-tagged NV p22 (**B**) or p22(AXΦA) (**C**) were fixed at 24 hpt and immuno-stained with antibody against SEAP (Alexa 594-conjugated secondary antibody) and the COPII marker protein Sec24C (Alexa 647-conjugated secondary antibody), stained with DAPI (blue fluorescence), and imaged by deconvolution microscopy. Channels were pseudo-colored as indicated for merged images. Inset in **B** represents an 8X zoom of the boxed region.
doi:10.1371/journal.pone.0013130.g008

Although all the effects of NV infection on the secretory pathway have not yet been explored, the results presented here demonstrate that, like PV 3A, direct antagonism of the secretory pathway is a cause, not an effect, of Golgi disassembly by p22. However, whereas at least two picornavirus 3A proteins interact with the cellular protein GBF-1 to inhibit COPI vesicle budding [13], NV p22 instead appears to target COPII vesicles with dependence upon a motif that is absent from picornavirus 3A proteins, suggesting that these two proteins take different approaches to the same ultimate outcome. It therefore appears that, like several picornaviruses [28,29], noroviruses encode two proteins, p22 and p48 (this study and [27]), with redundant functions of antagonizing the secretory pathway.

FCV p30, a homologue of p22, lacks an ER export signal and localizes exclusively to the ER when independently expressed ([26] and our unpublished observation). This is in line with the inability of BFA to inhibit FCV replication [24], as it does several picornaviruses, and further supports the notion that caliciviruses utilize a different architecture of cellular machinery for replication than do picornaviruses. A recent study has shown that MNV is also resistant to the cellular effects of BFA and does not have an effect on gross Golgi morphology [55]. It will therefore be interesting to determine the roles of p22 homologues from MNV and FCV in possible antagonism of ER/Golgi trafficking, as this would shed much light on similarities and differences between animal and human caliciviruses.

The biological significance of antagonism of the secretory pathway by p22 remains to be understood. This may facilitate viral pathogenesis rather than replication in a manner similar to the effect of the picornavirus 3A proteins that inhibit the immune response to virus-infected cells [14–16], ultimately leading to a more pathogenic infection [12]. Future study of the immune response to norovirus infection should consider secretory pathway antagonism by p22, as this protein may be key in deactivating interferon (IFN) and/or cytokine signaling following infection. Additionally, analysis of the cellular response to NV infection has demonstrated that NV is sensitive to IFN when exogenously added to cells replicating the NV genome [56,57]; however, NV does not induce the IFN pathway or IRF3 activation in Huh7 cells that support a single round of virus replication [58]. Although p22 may be contributing to a reduction in IFN release from cells, the possibility that p22 has additional inhibitory effects on the IFN pathway remains to be explored.

Since viruses utilize cellular processes and machinery for replication, understanding the mechanisms by which viruses parasitize the cell will both increase our understanding of these pathways and aid in the design of effective anti-viral countermeasures. The human norovirus nonstructural protein p22 encodes a novel and well-conserved motif that mimics a traditional di-acidic ER export signal. Instead of increasing the rate of protein trafficking in the secretory pathway, as is the normal function of these signals, the ER export signal mimic allows p22 to gain access to the secretory pathway, induce Golgi disassembly and inhibit cellular protein secretion. This is the first instance in which a pathogen has been described to use a motif similar to an ER export signal to ultimately inhibit cellular protein secretion. This motif constitutes a new target for the design of anti-viral drugs against noroviruses, as it is necessary for the antagonistic activity of p22 and is highly conserved in human noroviruses.

Materials and Methods

Vectors and cell lines

All genes were cloned using Gateway technology (Invitrogen) and expressed in pcDNA-DEST53 after sequence verification. Mutagenesis was performed using the QuikChange Multi Site-Directed Mutagenesis Kit (Stratagene). HEK-293T and Huh7 cells were maintained in DMEM supplemented with 10% fetal bovine serum. 293T cells were grown on plastic or coverslips coated with 10 μg/ml poly-D-lysine (Sigma). Transfection was carried out using Lipofectamine 2000 (Invitrogen) as per the manufacturer's instructions. cDNA encoding poliovirus 3A protein was obtained from Richard Lloyd of Baylor College of Medicine.

Transfection of NV RNA

NV RNA was purified from volunteer stool samples and transformed into Huh7 cells as described previously [30]. Briefly, virus was purified from volunteer stool samples by sucrose cushion and cesium chloride gradient extraction, following which viral RNA was extracted using the QIAamp Viral RNA Mini Kit (Qiagen) following the manufacturer's instructions. Five hundred nanograms of purified viral RNA were then transfected into cells, which were then cultured for the indicated period of time.

Immunofluorescence and antibodies

Cells were grown on cover slips and, following the indicated treatments, washed in PBS and subsequently fixed with 4% paraformaldehyde (Electron Microscopy Sciences, Hatfield, PA) in 0.1 M PBS and permeablized with 0.5% Triton X-100 in 0.1 M PBS. Cells were then washed in PBS and blocked with 1% bovine serum albumin (Sigma, St. Louis, MO) for 1 hour at 37°C, incubated overnight at 4°C with primary antibody in 0.1 M PBS, 1% BSA. Anti-human golgin-97 mouse monoclonal antibody was obtained from Molecular Probes (Invitrogen). GM130 mouse monoclonal antibody was obtained from BD Transduction Laboratories (San Jose, CA). Calnexin mouse monoclonal antibody and rabbit polyclonal antibody against β-COP were obtained from Affinity Bioreagents (Golden, CO). Rabbit polyclonal antibody against Sec24C was the generous gift of Bill Balch of Scripps Research Institute and has been previously described [59]. Rabbit polyclonal antibody against VP1 was also previously described [60]. Mouse monoclonal antibody 8B6 against placental alkaline phosphatase was obtained from AbCam (Cambridge, MA). Rabbit polyclonal antibody against protein disulfide isomerase (H-160) was obtained from Santa Cruz Biotechnology, Inc (Santa Cruz, CA). After incubation with primary antibody, cover slips were washed and incubated at room temperature for one hour with the corresponding AlexaFluor 488-, 594-, or 647-conjugated secondary antibodies (Invitrogen). Nuclei were stained with 300 nM DAPI (Invitrogen) at room temperature for 5 minutes. Cells were then washed and mounted using the ProLong Gold antifade reagent (Invitrogen). All images shown are representative of at least three independent experiments and the direct observation of

no less than 50 cells with GFP expression levels in approximately the middle 70th percentile.

Fluorescence deconvolution microscopy

Deconvolution microscopy was performed with a Zeiss AxioVert S100 TV microscope and a DeltaVison restoration microscopy system (Applied Precision, Inc.) and imaged using either a 63X objective lens (1.40 NA). A *z* series of focal planes was digitally imaged and deconvolved with the Delta-Vision constrained iterative algorithm to generate high-resolution images, from which Quick Projections were obtained. Brightness and contrast levels were adjusted appropriately in Adobe Photoshop version CS2.

Flow-coupled electron microscopy

293T cells were transfected with the indicated plasmids and at 24 hpt were harvested in 0.1 M PBS containing 1% BSA. Cells were then flow sorted for GFP on a BD SORP FACSAria II flow cytometric cell sorter with elution into 10% DMEM. Cells were then centrifuged at 500×g for 10 minutes, suspended in 10% DMEM and plated onto plastic dishes coated with 10 µg/ml poly-D lysine. Twenty-four hours later, and therefore 48 hpt, all cells were validated to be GFP positive under an epifluorescence microscope. Cells were then rinsed once in 0.1 M PBS and fixed in Karnovsky's Fixative (2% formaldehyde, 2.5% glutaraldehyde in 0.1 M cacodylate buffer +2 mM $CaCl_2$, pH 7.4) for 1 hour on ice. After being held overnight at 4°C in weak fix (1 part Karnovsky's Fixative: 10 parts 0.1 M cacodylate buffer +2 mM $CaCl_2$), the cells were rinsed 3 times in 0.1 M cacodylate buffer +2 mM $CaCl_2$, then post-fixed in 1% OsO_4 in 0.1 M cacodylate at 4°C. After 3 rinses in cacodylate buffer, cells were dehydrated in a gradient series of ethanols from 30–50%, en bloc stained with saturated uranyl acetate in 50% ethanol for 1 hour, carried through to 100% ethanol, then infiltrated in 1 part 100% ethanol: 1 part Spurr's Low Viscosity Resin overnight at room temperature. The rest of the infiltration was performed the next day, through 3 changes of pure resin. A small amount of pure resin was placed in the bottom of thoroughly drained plates, and the plated cells and resin were cured at 60°C for 3 days. Sections were cut at 70–80 nm using a Diatome diamond knife and an RMC MT6000-XL ultramicrotome. Sections were then collected on 100–150 mesh copper grids, counter-stained with Reynold's lead citrate and viewed on a Hitachi H-7500 transmission electron microscope. Image brightness and contrast were adjusted appropriately in Adobe Photoshop version CS2.

Cytosolic and membrane fractionation

Transfected 293T cells were suspended in 0.5 ml of homogenization buffer [200 mM HEPES (pH 7.5), 5 mM sodium pyrophosphate, 5 mM EGTA, 1 mM $MgCl_2$, 1 mM sodium orthovanadate, 50 µM leupeptin, 200 µM PMSF, 1 µM pepstatin A], followed by sonication and centrifugation at 100,000×g for one hour at 4°C, and the resulting supernatant was the cytosolic fraction. Pellets were resuspended in 0.5 ml extraction buffer [20 mM Tris-HCl (pH 7.5), 1% Triton X-100, 100 mM NaCl, 1 mM $MgCl_2$, 1 mM $CaCl_2$, 5 mM NaF, 1 mM sodium orthovanadate, 50 µM leupeptin, 200 µM PMSF, 1 µM pepstatin A], followed by incubation with rotation at 4°C for one hour and centrifuged at 100,000×g for 1 hour and the supernatant was collected as the membrane fraction. Fractions were then precipitated by addition of trichloroacetic acid to 10% and centrifugation at 16,000×g for 5 minutes. The pellet was then washed in acetone, pelleted, and resuspended in 50 µl of 5X SDS-PAGE sample buffer. Lysate aliquots were boiled for 3 minutes and analyzed by electrophoresis on 12.5% SDS-PAGE gels. Separated proteins were transferred from the gel to nitrocellulose membrane (Amersham Biosciences) and membranes were blocked in 5% Blotto (5% fat-free Carnation milk in 0.01 M PBS) and incubated with a mouse anti-GFP monoclonal antibody (Clontech, Mountain View, CA) in 0.5% Blotto overnight at RT. Primary antibody was removed and membranes were washed three times with 0.5% Blotto. Horseradish peroxidase-conjugated secondary goat anti-mouse immunoglobulin G antibody (Sigma-Aldrich) was incubated with the membranes for ~2 h at RT and subsequently washed three times with 0.5% Blotto. Membranes were developed with SuperSignal sensitivity substrate (Pierce).

SEAP assay

The plasmid pCMV-UTR-SEAP was obtained from J. Lindsay Whitton (Scripps Research Institute) [28] and was made into a Gateway-competent vector using the Gateway Vector Conversion System (Invitrogen) at the *NotI* site of the vector. 293T cells were grown to ~60% confluence in 24 well plates and transfected. Two hours before the indicated time points, cells were washed 2 times in 0.01 M PBS and the media was replaced with 400 µl of fresh media. At the indicated time points, the media containing "extracellular SEAP" was removed. At this same time point, "intracellular SEAP" values were obtained by washing cells once in cold 0.01 M PBS and adding 400 µl of media containing 0.5% Triton X-100 to lyse cells and solubilize any SEAP that had been retained in cells, and then incubating cells at room temperature for ~5 minutes. Lysed cells were then collected and spun at 13,000×g for one minute to remove cellular debris. Enzymatic SEAP activity in "intracellular" and "extracellular" fractions was assayed with the PhosphaLight TM System (Applied Biosystems), and overall Secreted SEAP was calculated with the equation: Secreted SEAP = $(SEAP_{extracellular}/(SEAP_{extracellular} + SEAP_{intracellular}))\times 100$ [28].

EndoH Sensitivity Assay

Sensitivity of VSV G and chimeras to digestion with endoglycosidase H was carried out as previously described [9,40,42] with minor modifications. VSV G or chimeras were expressed in 293T cells from the plasmid pMD2.G. Twenty-four hours post-transfection, cells were washed 3X in Cys/Met-free DMEM and incubated at 37°C for 15 minutes. Cells were then labeled with 200 µCi/ml ^{35}S-Met (Amersham BioSciences) for 15 minutes at 37°C, washed 3X in DMEM containing 10% FBS, and 400 µl of DMEM containing 10% FBS was added to cells, which were then incubated at 37°C. At the indicated time post-pulse, cells were washed 1X in cold PBS and harvested in VSV G Lysis Buffer (50 mM Tris pH 8, 62.5 mM EDTA, 1% NP-40, 0.4% deoxycholate, 50 µM leupeptin, 200 µM PMSF, 1 µM pepstatin A). Supernantants were cleared with 5 µl of Protein A Magnetic Beads (Invitrogen) and incubated overnight with monoclonal antibody against the luminal domain of VSV G (clone 8G5) [42], generously provided by Bill Balch, Scripps Research Institute. Immuno-complexes were collected by magnetic capture and washed 2X in VSV G Lysis Buffer, resuspended in 40 µl of 2.5X SDS-PAGE Sample Buffer and boiled for 5 minutes. Half of the IP was digested with 1 µl of endoglycosidase H (EndoH) (1 U/200 µl, Roche) at 37°C for 1 hour. EndoH treated and non-treated samples were then run on a 7.5% SDS-PAGE gel, transferred to nitrocellulose, and bands were quantitated following scanning on a Typhoon Trio Variable Mode Imager (GE Healthcare) and ImageQuant 5.1 to quantitate band intensity.

Statistical analysis

Two-tailed, unpaired Student's *t*-tests assuming unequal variance were used to determine statistical significance; p values are indicated where appropriate.

Supporting Information

Figure S1 NV p22 initially localizes to and induces disruption of the trans Golgi. Cells expressing GFP or GFP-tagged Norwalk virus (NV) p22 were immuno-stained for the trans Golgi marker protein golgin-97 (Alexa 594-conjugated secondary antibody, red fluorescence) at the indicated times post-transfection. Nuclei were stained with DAPI (blue fluorescence) and cells were imaged by deconvolution microscopy.
Found at: doi:10.1371/journal.pone.0013130.s001 (2.88 MB TIF)

Figure S2 Equivalent amounts of protein are made during SEAP analysis of p22 constructs containing alanine mutations within the predicted ER export signal. Proteins in lysates from the 36 hpt intracellular fraction of cells utilized in the indicated SEAP assay were run on a 4–20% SDS-PAGE gel and detected with monoclonal antibody against either GFP or actin by western blot.
Found at: doi:10.1371/journal.pone.0013130.s002 (0.74 MB TIF)

Figure S3 Calnexin is an appropriate marker of the endoplasmic reticulum in 293T cells. Non-transfected 293T cells were fixed and immuno-stained for the ER marker proteins calnexin and protein disulfide isomerase with mono- (red fluorescence, Alexa594-conjugated secondary antibody) and poly-clonal antibody (green fluorescence, Alexa488-conjugated secondary antibody), respectively. Nuclei were stained with DAPI (blue fluorescence) and cells were imaged by deconvolution microscopy.
Found at: doi:10.1371/journal.pone.0013130.s003 (3.02 MB TIF)

Acknowledgments

We gratefully acknowledge Debra Townley for assistance with electron microscopy. We also thank J. Lindsay Whitton and William Balch, both of Scripps Research Institute, for providing the pCMV-UTR-SEAP vector and VSV G monoclonal antibody, respectively. We also thank Richard Lloyd and Joseph Hyser of Baylor College of Medicine for critical manuscript review and helpful discussions.

Author Contributions

Conceived and designed the experiments: TMS SG KK SEC MKE. Performed the experiments: TMS SG. Analyzed the data: TMS SEC MKE. Contributed reagents/materials/analysis tools: KK. Wrote the paper: TMS MKE.

References

1. Scales SJ, Pepperkok R, Kreis TE (1997) Visualization of ER-to-Golgi transport in living cells reveals a sequential mode of action for COPII and COPI. Cell 90: 1137–1148.
2. Schekman R, Barlowe C, Yeung T, Hamamoto S, Hosobuchi D, et al. (1994) COPII - A Novel Coat Protein Required for Transport Vesicle Budding from the Endoplasmic-Reticulum. FASEB J 8: A1379.
3. Budnik A, Stephens DJ (2009) ER exit sites–localization and control of COPII vesicle formation. FEBS Lett 583: 3796–3803.
4. Tang BL, Wang Y, Ong YS, Hong WJ (2005) COPII and exit from the endoplasmic reticulum. Biochimica et Biophysica Acta-Mol Cell Res 1744: 293–303.
5. Saraste J, Dale HA, Bazzocco S, Marie M (2009) Emerging new roles of the pre-Golgi intermediate compartment in biosynthetic-secretory trafficking. FEBS Lett 583: 3804–3810.
6. Polishchuk RS, Capestrano M, Polishchuk EV (2009) Shaping tubular carriers for intracellular membrane transport. FEBS Lett 583: 3847–3856.
7. Nakamura N, Yamazaki S, Sato K, Nakano A, Sakaguchi M, et al. (1998) Identification of potential regulatory elements for the transport of Emp24p. MBC 9: 3493–3503.
8. Giraudo CG, Maccioni HJF (2003) Endoplasmic reticulum export of glycosyltransferases depends on interaction of a cytoplasmic dibasic motif with sar1. Mol Biol Cell 14: 3753–3766.
9. Nishimura N, Balch WE (1997) A di-acidic signal required for selective export from the endoplasmic reticulum. Science 277: 556–558.
10. Nishimura N, Bannykh S, Slabough S, Matteson J, Altschuler Y, et al. (1999) A di-acidic (DXE) code directs concentration of cargo during export from the endoplasmic reticulum. J Biol Chem 274: 15937–15946.
11. Chardin P, McCormick F (1999) Brefeldin A: the advantage of being uncompetitive. Cell 97: 153–155.
12. Wessels E, Duijsings D, Niu TK, Neumann S, Oorschot VM, et al. (2006) A viral protein that blocks Arf1-mediated COP-I assembly by inhibiting the guanine nucleotide exchange factor GBF1. Dev Cell 11: 191–201.
13. Wessels E, Duijsings D, Lanke KHW, van Dooren SHJ, Jackson CL, et al. (2006) Effects of picornavirus 3A proteins on protein transport and GBF1-dependent COP-I recruitment. J Virol 80: 11852–11860.
14. Deitz SB, Dodd DA, Cooper S, Parham P, Kirkegaard K (2000) MHC I-dependent antigen presentation is inhibited by poliovirus protein 3A. Proc Natl Acad Sci U S A 97: 13790–13795.
15. Dodd DA, Giddings TH, Kirkegaard K (2001) Poliovirus 3A protein limits interleukin-6 (IL-6), IL-8, and beta interferon secretion during viral infection. J Virol 75: 8158–8165.
16. Neznanov N, Kondratova A, Chumakov KM, Angres B, Zhumabayeva B, et al. (2001) Poliovirus protein 3A inhibits tumor necrosis factor (TNF)-induced apoptosis by eliminating the TNF receptor from cell surface. J Virol 75: 10409–10420.
17. Mead PS, Slutsker L, Dietz V, Mccaig LF, Bresee JS, et al. (1999) Food-related illness and death in the United States. EID 5: 607–625.
18. Glass RI, Parashar U, Estes MK (2009) Norovirus gastroenteritis. N Engl J Med 361: 50–59.
19. Estes MK, Prasad BVV, Atmar RL (2006) Noroviruses everywhere: has something changed? Curr Opin Infect Dis 19: 467–474.
20. Blanton LH, Adams SM, Beard RS, Wei G, Bulens SN, et al. (2006) Molecular and epidemiologic trends of caliciviruses associated with outbreaks of acute gastroenteritis in the United States, 2000–2004. J Infect Dis 193: 413–421.
21. Siebenga JJ, Vennema H, Duizer E, Koopmans MPG (2007) Gastroenteritis caused by norovirus GGII.4, the Netherlands, 1994-2005. EID 13: 144–146.
22. Hardy ME (2005) Norovirus protein structure and function. FEMS Microbiol Lett 253: 1–8.
23. Matsui SM, Kim JP, Greenberg HB, Su W, Sun Q, et al. (1991) The isolation and characterization of a Norwalk virus-specific cDNA. J Clin Invest 87: 1456–1461.
24. Green KY, Mory A, Fogg MH, Weisberg A, Belliot G, et al. (2002) Isolation of enzymatically active replication complexes from feline calicivirus-infected cells. J Virol 76: 8582–8595.
25. Wobus CE, Karst SM, Thackray LB, Chang KO, Sosnovtsev SV, et al. (2004) Replication of Norovirus in cell culture reveals a tropism for dendritic cells and macrophages. PLoS Biol 2: 2076–2084.
26. Bailey D, Kaiser WJ, Hollinshead M, Moffat K, Chaudhry Y, et al. (2010) Feline calicivirus p32, p39 and p30 proteins localize to the endoplasmic reticulum to initiate replication complex formation. J Gen Virol 91: 739–749.
27. Fernandez-Vega V, Sosnovtsev SV, Belliot G, King AD, Mitra T, et al. (2004) Norwalk virus N-terminal nonstructural protein is associated with disassembly of the Golgi complex in transfected cells. J Virol 78: 4827–4837.
28. Cornell CT, Kiosses WB, Harkins S, Whitton JL (2006) Inhibition of protein trafficking by coxsackievirus B3: Multiple viral proteins target a single organelle. J Virol 80: 6637–6647.
29. Doedens JR, Kirkegaard K (1995) Inhibition of Cellular Protein Secretion by Poliovirus Proteins 2B and 3A. EMBO J 14: 894–907.
30. Guix S, Asanaka M, Katayama K, Crawford SE, Neill FH, et al. (2007) Norwalk virus RNA is infectious in mammalian cells. J Virol 81: 12238–12248.
31. Persico A, Cervigni RI, Barretta ML, Colanzi A (2009) Mitotic inheritance of the Golgi complex. FEBS Lett 583: 3857–3862.
32. Zaal KJM, Smith CL, Polishchuk RS, Altan N, Cole NB, et al. (1999) Golgi membranes are absorbed into and reemerge from the ER during mitosis. Cell 99: 589–601.
33. Green KY (2007) Caliciviridae: The Noroviruses. In: Knipe DM, Howley PM, eds. Fields Virology. Philadelphia: Lippincott Williams & Wilkins. pp 949–980.
34. Doedens JR, Giddings TH, Kirkegaard K (1997) Inhibition of endoplasmic reticulum-to-Golgi traffic by poliovirus protein 3A: Genetic and ultrastructural analysis. J Virol 71: 9054–9064.
35. Berger J, Hauber J, Hauber R, Geiger R, Cullen BR (1988) Secreted Placental Alkaline-Phosphatase - A Powerful New Quantitative Indicator of Gene-Expression in Eukaryotic Cells. Gene 66: 1–10.
36. Choe SS, Dodd DA, Kirkegaard K (2005) Inhibition of cellular protein secretion by picornaviral 3A proteins. Virology 337: 18–29.
37. Rost B, Fariselli P, Casadio R (1996) Topology prediction for helical transmembrane proteins at 86% accuracy. Protein Sci 5: 1704–1718.
38. Fujita K, Krishnakumar SS, Franco D, Paul AV, London E, et al. (2007) Membrane topography of the hydrophobic anchor sequence of poliovirus 3A and 3AB proteins and the functional effect of 3A/3AB membrane association upon RNA replication. Biochemistry 46: 5185–5199.

39. Zheng DP, Ando T, Fankhauser RL, Beard RS, Glass RI, et al. (2006) Norovirus classification and proposed strain nomenclature. Virology 346: 312–323.
40. Sevier CS, Weisz OA, Davis M, Machamer CE (2000) Efficient export of the vesicular stomatitis virus G protein from the endoplasmic reticulum requires a signal in the cytoplasmic tail that includes both tyrosine-based and di-acidic motifs. Mol Biol Cell 11: 13–22.
41. Paulhe F, Imhof BA, Wehrle-Haller B (2004) A specific endoplasmic reticulum export signal drives transport of stem cell factor (Kitl) to the cell surface. J Biol Chem 279: 55545–55555.
42. Tisdale EJ, Bourne JR, Khosravifar R, Der CJ, Balch WE (1992) Gtp-Binding Mutants of Rab1 and Rab2 Are Potent Inhibitors of Vesicular Transport from the Endoplasmic-Reticulum to the Golgi-Complex. J Cell Biol 119: 749–761.
43. Wessels E, Duijsings D, Lanke KHW, Melchers WJG, Jackson CL, et al. (2007) Molecular determinants of the interaction between coxsackievirus protein 3A and guanine nucleotide exchange factor GBF1. J Virol 81: 5238–5245.
44. Beske O, Reichelt M, Taylor MP, Kirkegaard K, Andino R (2007) Poliovirus infection blocks ERGIC-to-Golgi trafficking and induces microtubule-dependent disruption of the Golgi complex. J Cell Sci 120: 3207–3218.
45. Barr FA, Short B (2003) Golgins in the structure and dynamics of the Golgi apparatus. Curr Opin Cell Biol 15: 405–413.
46. Short B, Haas A, Barr FA (2005) Golgins and GTPases, giving identity and structure to the Golgi apparatus. Biochim Biophys Acta 1744: 383–395.
47. Strating JR, Martens GJ (2009) The p24 family and selective transport processes at the ER-Golgi interface. Biol Cell 101: 495–509.
48. Lev S, Ben Halevy D, Peretti D, Dahan N (2008) The VAP protein family: from cellular functions to motor neuron disease. Trends Cell Biol 18: 282–290.
49. Ettayebi K, Hardy ME (2003) Norwalk virus nonstructural protein p48 forms a complex with the SNARE regulator VAP-A and prevents cell surface expression of vesicular stomatitis virus G protein. J Virol 77: 11790–11797.
50. Kim J, Thanabalasuriar A, Chaworth-Musters T, Fromme JC, Frey EA, et al. (2007) The bacterial virulence factor NleA inhibits cellular protein secretion by disrupting mammalian COPII function. Cell Host Microbe 2: 160–171.
51. Rismanchi N, Puertollano R, Blackstone C (2009) STAM Adaptor Proteins Interact with COPII Complexes and Function in ER-to-Golgi Trafficking. Traffic 10: 201–217.
52. Mukherjee S, Chiu R, Leung SM, Shields D (2007) Fragmentation of the Golgi apparatus: an early apoptotic event independent of the cytoskeleton. Traffic 8: 369–378.
53. Teterina NL, Bienz K, Egger D, Gorbalenya AE, Ehrenfeld E (1997) Induction of intracellular membrane rearrangements by HAV proteins 2C and 2BC. Virology 237: 66–77.
54. Konan KV, Giddings TH, Ikeda M, Li K, Lemon SM, et al. (2003) Nonstructural protein precursor NS4A/B from hepatitis C virus alters function and ultrastructure of host secretory apparatus. J Virol 77: 7843–7855.
55. Hyde JL, Sosnovtsev SV, Green KY, Wobus C, Virgin HW, et al. (2009) Mouse norovirus replication is associated with virus-induced vesicle clusters originating from membranes derived from the secretory pathway. J Virol 83: 9709–9719.
56. Chang KO, Sosnovtsev SV, Belliot G, King AD, Green KY (2006) Stable expression of a Norwalk virus RNA replicon in a human hepatoma cell line. Virology 353: 463–473.
57. Chang KO, George DW (2007) Interferons and ribavirin effectively inhibit Norwalk virus replication in replicon-bearing cells. J Virol 81: 12111–12118.
58. Guix S, Estes MK (2009) Caliciviridae and Astroviridae. In: Brasier AR, Garcia-Sastre A, Lemon SM, eds. Cellular Signaling and Innate Immune Responses to RNA Virus Infections. Washington D.C.: ASM Press. pp 389–402.
59. Aridor M, Weissman J, Bannykh S, Nuoffer C, Balch WE (1998) Cargo selection by the COPII budding machinery during export from the ER. J Cell Biol 141: 61–70.
60. Gilpatrick SG, Schwab KJ, Estes MK, Atmar RL (2000) Development of an immunomagnetic capture reverse transcription-PCR assay for the detection of Norwalk virus. J Virol Methods 90: 69–78.

Biosci. Biotechnol. Biochem., **74** (3), 541–547, 2010

Binding of Norovirus Virus-Like Particles (VLPs) to Human Intestinal Caco-2 Cells and the Suppressive Effect of Pasteurized Bovine Colostrum on This VLP Binding

Kosuke MURAKAMI,[1] Sayaka SUZUKI,[1] Naohito AOKI,[2] Tetsuya OKAJIMA,[3] Daita NADANO,[1] Kenji UCHIDA,[4] Kousaku YAMASHITA,[4] Tomoichiro OKA,[5] Kazuhiko KATAYAMA,[5] Naokazu TAKEDA,[5] and Tsukasa MATSUDA[1,†]

[1]*Department of Applied Molecular Biosciences, Graduate School of Bioagricultural Sciences, Nagoya University, Nagoya, Aichi 464-8601, Japan*
[2]*Department of Life Science, Graduate School of Bioresources, Mie University, Tsu, Mie 514-8507, Japan*
[3]*Department of Biochemistry II, Graduate School of Medicine, Nagoya University, Nagoya, Aichi 466-0065, Japan*
[4]*Central R&D Laboratory, Kobayashi Pharmaceutical Co., Ltd., Ibaraki, Osaka 567-0057, Japan*
[5]*Department of Virology II, National Institute of Infectious Diseases, Musashimurayama, Tokyo 208-0011, Japan*

Received October 5, 2009; Accepted December 3, 2009; Online Publication, March 7, 2010
[doi:10.1271/bbb.90729]

Noroviruses (NoVs), which cannot be grown in cell culture, are a major infectious agent of gastroenteritis. An *in vitro* assay system was established for the evaluation of NoV binding to enterocytes using virus-like particles (VLPs) produced in a baculovirus system expressing a NoV VP1 capsid protein. After confirmation of the purity by MS analysis, VLPs were incubated with human intestinal Caco-2 cells. NoV VLPs were detected clearly by confocal laser microscopy only on a certain population of Caco-2 cells, and were semi-quantified by immunoblotting of cell lysates. Then the suppressive effect of pasteurized bovine colostrum was analyzed on the VLP binding to Caco-2 cells by immunoblotting. The colostrum reduced VLP binding in a dose-dependent manner, at about 50% suppression with 12.5 μg of the colostral proteins. Furthermore, the colostrum contained IgG antibodies reacting to VLPs, suggesting that cross-reactive antibodies in the bovine colostrums block human NoV binding to intestinal cells.

Key words: food intoxication (poisoning); nonbacterial gastroenteritis; colostral immunoglobulin; natural antibody

Noroviruses (NoVs) are major etiological agents of human nonbacterial infectious gastroenteritis, including food intoxication.[1)] Human NoVs are non-cultivable so far in that the viruses cannot be grown and replicated in cell culture systems,[2)] resulting in limited information on the infection and replication mechanisms of human NoVs. However, development of recombinant virus-like particles (VLPs) has supplied a new experimental tool for studies of interactions between human NoVs and host cells.[3)] An approximately 60-kDa capsid protein, VP1, expressed in recombinant baculovirus systems is believed to self-assemble spontaneously into VLPs 38 nm in diameter.[4)] These VLPs have been reported to be morphologically and antigenically similar to the native virions,[5)] and are regarded as empty virus particles without a virus genome.

The molecules responsible for NoV binding to host cells at the initial infection step have been searched for using NoV VLPs. Some natural and synthesized carbohydrate chains forming human histo-blood group antigens have been found to bind to NoV VLPs *in vitro*, *e.g.*, by ELISA using anti-VLPs antibodies.[6)] On the other hand, VLP binding to host cells has been investigated using metabolically radio-labeled NoV VLPs, and human intestinal Caco-2 cells were reported to be the most remarkable in the VLP binding among several cell lines, including human intestinal epithelial and embryonic kidney cells and insect fibroblastic cells,[3)] but no microscopic images showing VLP binding to Caco-2 cells have been reported. Heparan sulfate and an unidentified 105-kDa protein of Caco-2 cells were found to be possible receptors for NoV VLPs in studies using radio-labeled NoV VLPs.[7,8)] The human intestinal Caco-2 cell line is known to differentiate morphologically and functionally in confluent culture and resembles epithelial cells of small intestine[9)] despite its colon-cancer origin.[10)]

Breast milk plays important roles in supplying not only nutrients but also immunity against environmental pathogens. Especially, a special milk, termed colostrum, produced by the mammary glands in late pregnancy, is believed to be critical for neonates to grow healthy until their development of own immune systems.[11)] Colostrum from ruminant animals, including bovine ones, is different from that of humans in that bovine colostrum contains a large amount of IgG antibodies,[12)] which are absorbed by neonates in intact form across the intestinal epithelium, because the mother's serum IgGs are not delivered to the fetal circulation *via* the placenta and umbilical cord.[13)] On the other hand, human breast milk, including colostrum, contains secretory IgA antibodies, which play important roles in preventing the coloniza-

† To whom correspondence should be addressed. Fax: +81-52-789-4128; E-mail: tmatsuda@agr.nagoya-u.ac.jp

Abbreviations: NoV, norovirus; SaV, sapovirus; VLP, virus-like particle; P-Col, pasteurized colostrum; R-milk, raw milk; R-Col, raw colostrum; MALDI-TOF, matrix-assisted laser-desorption ionization-time of flight

tion of pathogenic bacteria at the intestinal mucus epithelium.[14] In general, the biological definition of colostrum is breast milk that is synthesized and accumulated in mammary glands during the last stage of pregnancy and secreted within 1 d of giving birth. However, in Japan, bovine milk obtained within 5 d of delivery is regarded to be colostrum as a matter of regulation without definite scientific basis, and may not be used as a food.

The first aim of the present study was to establish *in vitro* assay systems to estimate NoV binding to the intestinal epithelium using non-radio-labeled VLPs and cultured Caco-2 cells, and the second was to evaluate the potential suppressive effects of bovine colostrum on NoV binding to the intestinal epithelium using established assay methods. Immunofluorescence staining of Caco-2 cells and immunoblotting analysis of the cell lysates clearly indicated that NoV VLPs bound to Caco-2 cells, and that the detection sensitivity in the established assay was comparable to that of previously reported methods using radio-labeled VLPs. Moreover, bovine colostrum obtained from healthy lactating cows at 6 or 7 d after parturition suppressed VLP binding to Caco-2 cells and contained IgGs cross-reactive to human NoV VLPs.

Materials and Methods

Bovine colostrums. Pasteurized and dried bovine colostrums were prepared at an industrial level in the facility of Kobayashi Pharmaceuticals (Osaka, Japan). For preparation of the pasteurized colostrum (P-Col), colostrums were collected from healthy lactating cows (Holstein) at 6 or 7 d after parturition and pooled. The pooled colostrums were defatted by centrifugation, pasteurized by heating at 72 °C for 15 s (an HTST condition), and concentrated by ultrafiltration, followed by spray-drying under low heating conditions. The powdered P-Col consisted of 49.8% protein, 36.4% lactose, 1.8% fat, 7.8% minerals, and 4.2% moisture. On the other hand, in the preparation of raw milk and colostrum samples (R-Milk and R-Col respectively), milk and colostrums were collected from mid-lactation (2–4 months after parturition) and early-lactation (36–48 h after parturition) healthy Holstein cows respectively bred at a local dairy farm (the Shimizu farm, Kariya, Japan). The R-Milk and R-Col samples were defatted by centrifugation and kept frozen at −20 °C until use.

Preparation of VLPs. VLPs of NoV (Ueno-7k strain) were produced by means of a baculovirus expression system, in which a recombinant VP1 capsid protein of NoV was overexpressed in an insect cell line, High Five™ (Invitrogen), the VLPs secreted into the cell medium were collected by ultracentrifugation at 30,000 rpm using an SW32 rotor (Beckman, Fullerton, CA), and the 38-nm VLPs of native virion size were purified by ultracentrifugation in CsCl containing solution.[15] The size and purity of the VLP preparation were confirmed by electron microscopy. Sapovirus (SaV) VLPs (NK24 strain) were prepared as described previously.[16]

SDS–PAGE and immunoblotting. Sodium dodecyl sulfate-polyacrylamide gel electrophoresis (SDS–PAGE) was performed by the method of Laemmli.[17] The protein samples were boiled for 3 min in SDS–PAGE sample buffer in the presence of 2-mercaptoethanol. Protein bands in gels were detected with Coomassie Brilliant Blue R-250 (CBB) staining. In immunoblotting, the separated proteins were blotted onto a poly (vinylidene difluoride) (PVDF) membrane (Immobilon; Millipore, Bedford, MA), and were visualized using anti-NoV VLP antibody[18] using an enhanced chemiluminescence (ECL) system, as described previously.[19] The relative intensity of the immune-stained band for VP1 was analyzed semi-quantitatively by densitometric measurement using the Light Capture system and CS analyzer software version 3 (Atto Instruments, Tokyo).

Protein identification by MS analysis. The protein bands of the VLP preparation detected by CBB staining of SDS-polyacrylamide gel were excised, cut into small pieces, and subjected to the in-gel digestion. After they were destained with a 50% acetonitrile/25 mM NH_4HCO_3 mixture, the gel pieces were dehydrated with 100 µl of acetonitrile, dried by vacuum centrifugation, and then rehydrated in buffer containing 25 mM NH_4HCO_3 and 1.1 units of trypsin (Trypsin Gold, MS Grade, Promega). Following digestion for 17 h at 37 °C, the peptides were extracted from the gel stepwise with 0.1% trifluoroacetic acid, a 0.1% trifluoroacetic acid/50% acetonitrile mixture, and 100% acetonitrile. The pooled extract was concentrated by vacuum centrifugation and desalted by ZipTip µ-C18 (Millipore). The extracted peptides were subjected to MALDI (matrix-assisted laser-desorption ionization) TOF (time of flight) mass spectrometry using a 4700 Proteomics Analyzer (Applied Biosystems), as described previously.[20] The MS and MS/MS data were analyzed using Mascot software (Matrix Science, London).

Cell culture and VLP binding assay. Caco-2 cells from the American Type Culture Collection (Rockville, MD) were maintained in DMEM supplemented with 10% heat inactivated fetal calf serum (Sigma-Aldrich, St. Louis, MO), 1% nonessential amino acids solution (Sigma), 100 U/ml of penicillin, and 100 µg/ml of streptomycin, and grown under humidified 5% CO_2 and 95% air at 37 °C. For the immunoblotting analysis, Caco-2 cells were seeded at 1.0×10^5 cells/cm^2 in 48-well culture plates (Corning, NY) and cultured for 3 d in DMEM supplemented with 10% FCS at 37 °C in a humidified atmosphere with 5% CO_2. Then the cells in each well were washed with cold DMEM and incubated with various concentrations of VLPs in DMEM at 4 °C for 1 h. After washing with cold DMEM 3 times, the cells were lysed with Laemmli buffer. After centrifugation, the supernatants were collected as cell lysates and subjected to immunoblotting analysis, as described above. African green monkey kidney cells, COS7, were cultured and treated similarly with VLPs as a negative control.

Immunofluorescence microscopy. Caco-2 cells were seeded at 1.0×10^5 cells/cm^2 onto type-I-collagen-coated coverslips in the 6-well culture plate and cultured for 3 d in DMEM supplemented with 10% FCS at 37 °C under a humidified atmosphere with 5% CO_2. Then the cells on coverslips were washed with cold PBS and incubated with various concentrations of VLPs in DMEM at 4 °C for 1 h. After washing with cold DMEM 3 times, the cells were fixed with 4% paraformaldehyde in PBS for 30 min on ice, washed with DMEM, and blocked with NETG (150 mM NaCl, 5 mM EDTA, 50 mM Tris–HCl, 0.05% Triton X-100, and 0.25% gelatin). The cells were incubated with NETG containing the rabbit anti-NoV VLP for VLPs[18] or mouse anti-ZO1 (Zymed) for a cell-tight junction, and subsequently with NETG containing Alexa Fluor® 568 goat anti-rabbit IgG (Molecular Probes, Eugene, OR) or Alexa Fluor® 488 goat anti-mouse IgG (Molecular Probes) for 1 h at room temperature under darkness. The cells were stained with TOTO-3 (Molecular Probes) too for nuclear staining. After washing with PBS, the cells on coverslips were mounted onto glass slides containing a drop of 50% glycerol in PBS. Imaging was performed on a Zeiss Axioplan2 microscope equipped with a LSM5 PASCAL laser scanning confocal optics (Carl Zeiss, Thornwood, NY) in multi-track mode.

ELISA. IgG antibodies specific for NoV and SaV VLPs in bovine colostrums were measured by ELISA, as described previously.[21] Briefly, 96-well plates (Nunc, Roskilde) were coated with 1 µg per well of VLPs in PBS. After washing and blocking, the plates were incubated with colostrums diluted to a 1–20 µg protein concentration with PBS/Tween/BSA, washed with PBS/Tween, and incubated with POD-conjugated anti-bovine IgG (H and L chains) antibody (Abcam, Cambridge).

Results

NoV VLPs specifically bound to a certain population of Caco-2 cells

The NoV VLPs used in the cell-binding assay were concentrated and purified by ultracentrifugation from culture supernatants of the infected insect cells. The

A

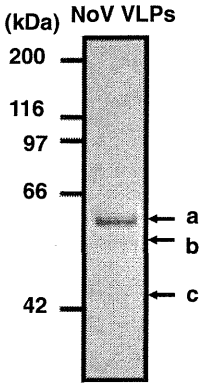

B

Band	Protein	MSDB Accession #	Score MS	Score MS/MS	Molecular weight
a	Capsid protein - Norwalk-like virus	Q8JW42_9CALI	132	416	60709
b	Capsid protein - Norwalk-like virus	Q8JW42_9CALI	133	181	60709
c	Capsid protein - Norwalk-like virus	Q8JW42_9CALI	90	104	60709

C

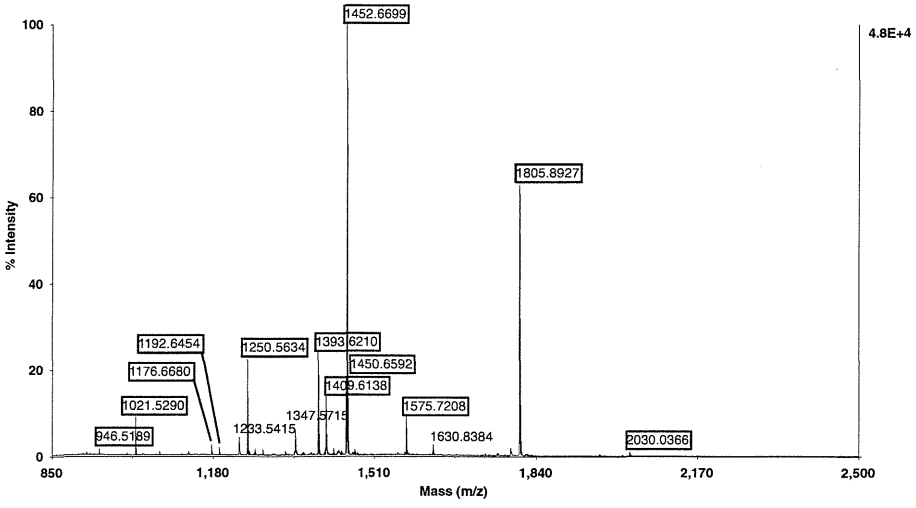

Fig. 1. SDS–PAGE and MS Analysis of NoV VLPs.

NoV VLPs (1 μg) were subjected to SDS–PAGE, followed by CBB staining (A). Each protein band (a, b, and c, indicated by arrows) was excised, in-gel digested with trypsin, and subjected to MALDI-TOF/MS analysis. All protein bands were identified as the capsid protein, VP1, of NoVs, previously termed Norwalk viruses (B) based on MS data analyzed using the Mascot software. The MS of band c is shown as a representative (C), in which mass peaks identified as VP1 are marked with open squares.

purity of the VLP preparation was examined by SDS–PAGE and subsequent MS analysis. The NoV VLP preparation gave a single major band of 60 kDa, a faint band of 57 kDa, and a nearly invisible 45-kDa band (Fig. 1A). All three protein bands were identified as intact VP1 and fragments of it by MS analysis (Fig. 1B) and their estimated molecular mass by SDS–PAGE was determined. As found in a representative mass spectrum of the 45-kDa band, most of the tryptic peptide signals were assigned to theoretical tryptic peptides of the NoV capsid protein, VP1 (Fig. 1C).

To elucidate the binding of NoV VLPs to human intestinal Caco-2 cells, an immunofluorescence microscopic approach was applied to cells incubated with the VLPs of NoV and of SaV for comparison. As shown in Fig. 2A and B, fluorescent signals of NoV VLPs were clearly detected by confocal laser scanning microscopy in several restricted cells, which formed colonies in the cell culture wells, whereas no signals of SaV VLPs were detected under the same conditions. The difference in the fluorescent signal was clear between VLP-binding positive and negative cells. Non-specific binding of the antibodies to NoV and SaV VLPs was not observed in the cells without VLP treatment. A representative three-dimensional image of a magnified field clearly indicated that NoV VLPs bound to almost the whole area of the apical cell surface of the positive cells (X/Y and Y/Z planes of Fig. 2C), whereas none did to any area of the negative cells (X/Y and X/Z planes of Fig. 2C).

The binding of NoV VLPs to Caco-2 cells was analyzed in more detail by immunoblotting of total cell lysates. Caco-2 cells and COS7 cells as a negative control were incubated with the VLPs (100 ng) for various periods of time up to 180 min. Immunostained VP1 band of Caco-2 cell lysates became detectable after 5 min of incubation, and the band intensity increased with incubation time, whereas that of COS7 lysates was faintly detected only in the sample of 180 min of incubation (Fig. 3A). Based on the band intensity obtained by densitometric analysis, the NoV VLPs bound to the Caco-2 cells in a well at 180 min of incubation was estimated to be about 16 ng (data not shown). To estimate the binding affinity of VLPs to Caco-2 cells as well as the detection sensitivity of bound VLPs by immunoblotting, various amounts (5 to 150 ng per well) of VLPs were incubated with Caco-2 cells, and were subjected to immunoblotting analysis. The VP1 band was clearly detected at levels of 75 ng or more in a dose-dependent manner, and it was still detectable when only 5 ng of VLPs was incubated with Caco-2 cells (Fig. 3B).

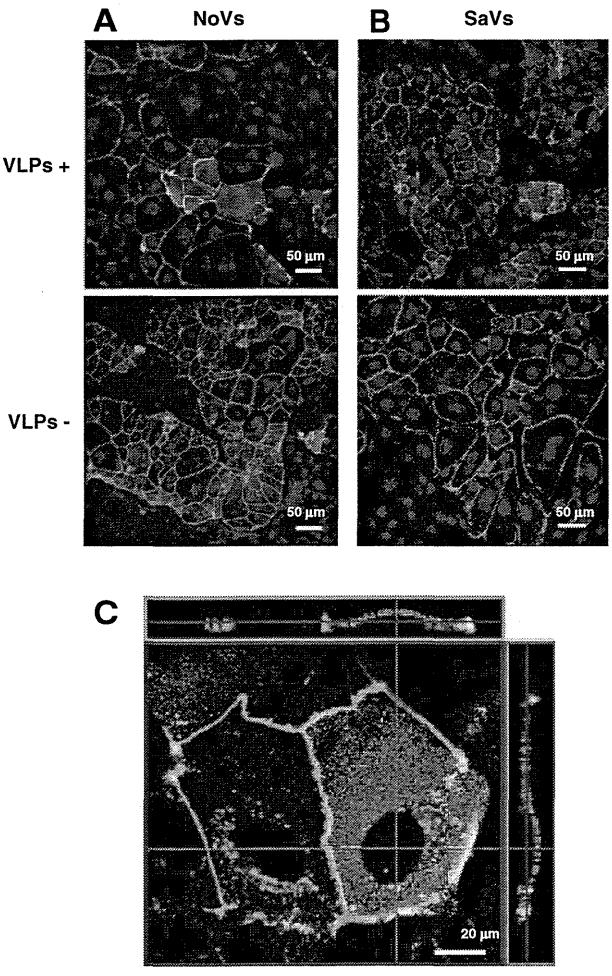

Fig. 2. Confocal Laser Scanning Microscopy of Caco-2 Cells Incubated with NoV and SaV VLPs.

Caco-2 cells were cultured for 3 d on type-I-collagen-coated coverslips in a 6-well culture plate and incubated for 1 h at 4 °C with (+) and without (−) 0.5 μg of NoV VLPs (A and C) or SaV VLPs (B). After washing and paraformaldehyde fixation, the cells were stained with rabbit anti-NoV VLP, rabbit anti-SaV VLP, and mouse anti-ZO-1 (a tight junction marker) antibodies, and subsequently with Alexa Fluor 568 goat anti-rabbit IgG or Alexa Fluor 488 goat anti-mouse IgG. Nuclei were stained with TOTO-3. Typical Z-axis images of Caco-2 cells incubated with NoV VLPs were constructed digitally in the XZ and YZ planes, shown as horizontal and vertical lines in the XY plane (C). Red, NoV VLPs; green, ZO-1; blue, nuclear. Bars, 50 μm in panels A and B; 20 μm in panel C.

Pasteurized bovine colostrums suppressed VLP-binding to Caco-2 cells and contained anti-NoV IgG

Utilizing the above described assay system, the suppressive effect of P-Col on NoV VLP-binding to Caco-2 cells was examined semi-quantitatively by immunoblotting. As shown in Fig. 4A, pre-incubation of the VLPs with an excess amount (25 μg protein against 0.1 μg of VLPs) of P-Col markedly decreased the band intensity of the VLPs in the Caco-2 cell lysate. Non-specific staining was not observed in either lysate of the cells incubated with the various protein concentrations of the colostrums without VLPs. The VP1 band intensity in each cell lysate was quantified by densitometric analysis (Fig. 4B), indicating that the VLPs binding to Caco-2 cells decreased gradually with increases in the amount of P-Col used in pre-incubation with VLPs, and 50% suppression was achieved with 12.5 μg of P-Col.

Bovine colostrums are known to contain large amounts of IgG. The content of the intact form of IgG consisting of two heavy and two light chains in P-Col and R-Col was estimated by SDS–PAGE under non-reduced conditions, to which various amounts (equivalent to 15–50 μg protein) of each sample were subjected (Fig. 5A). The 200-kDa band was identified as IgG by MS and immunoblotting analysis (data not shown), and it was the most dominant protein component in both R-Col and P-Col. The IgG content estimated from the band intensity was higher in P-Col than in R-Col. This higher IgG proportion of P-Col might be ascribed to the preferential concentration of IgG and other proteins during the heat pasteurization process, including the ultrafiltration described in "Materials and Methods."

Bovine IgG antibodies with reactivity to human NoV VLPs were examined by ELISA on P-Col as well as R-Col and R-Milk for comparison (Fig. 5B). Anti-NoV VLP IgG was detected remarkably not only in R-Col but also in P-Col, while R-Milk showed almost no IgG-binding activity to the VLPs. The IgG reactivity to NoV VLPs of P-Col was a little higher than that of R-Col. VLP binding activity in P-Col was analyzed more in detail at various protein-concentrations using VLPs of SaV in addition to NoV, which belong to the same Calicivirus family. As shown in Fig. 5C, the IgG antibodies in P-Col were reactive to VLPs not only of NoV but also of SaV, and the ELISA value increased in a manner dependent on the sample protein concentration. The rabbit antibody raised by immunizing with NoV VLPs did not cross-react with SaV VLPs under either ELISA or immunoblotting analysis (data not shown).

Discussion

A single VLP is believed to be constructed by spontaneous association of 180 molecules of a single capsid protein, VP1, and the structural or architectural similarity to virus virions has been demonstrated by X-ray crystallography.[22] Moreover, antibodies prepared by immunizing animals with VLPs react well with virus virions in patients' specimens, and thus immunochemical detection of etiological agents became possible in diagnosis for NoV food poisoning. Hence, the morphological and immunochemical properties of VLPs have been investigated, while the components of VLPs have not been well characterized biochemically. In the present study, the purity and intactness of VLPs were analyzed by SDS–PAGE and MS-based protein identification, in which all of one major and two minor proteins were identified to be VP1 (Fig. 1). This indicates that the VLPs prepared by the baculovirus expression system are constructed from a single capsid protein, VP1, as expected, without contaminating proteins from the expression system, but a trace amount of degraded VP1 was also present in the VLPs. Nevertheless, such a faint proteolysis of VP1 is expected not to affect the VLPs-cells binding assay, and therefore the VLP preparation was used in the binding assay. It is unlikely that the degraded VP1 or partially degraded VLPs inhibited the binding of intact VLPs to the cells.

A recent study on NoV infection using biopsy specimens from the duodenum of patients with NoV

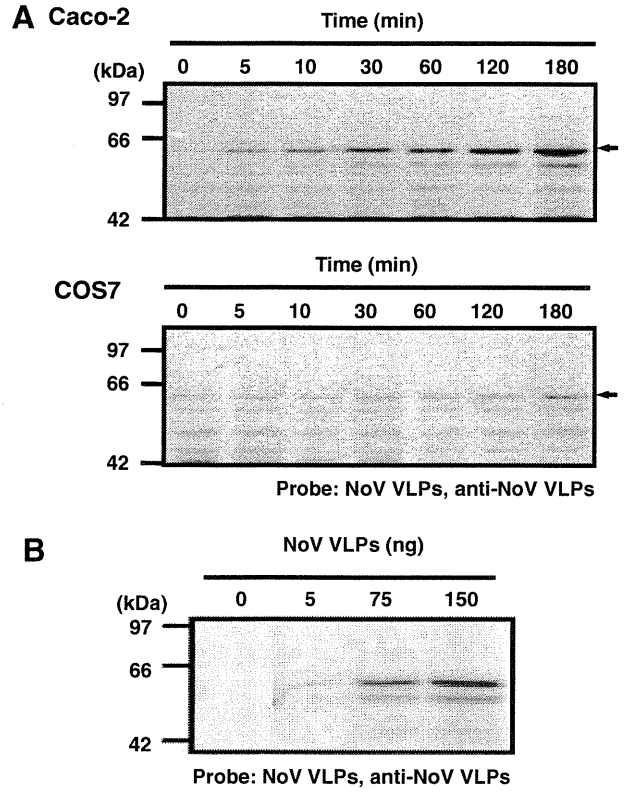

Fig. 3. Immunoblotting Analysis of NoV VLPs Bound to Caco-2 Cells.

Caco-2 cells were cultured in 48-well culture plates for 3 d and then incubated with NoV VLPs (0.1 μg per well) at 4 °C for various periods (5–180 min). Total cell lysates were subjected to SDS–PAGE, followed by immunoblotting for NoV VP1 (A). The migration position of NoV VP1 is indicated by arrows. The cells were incubated with various amounts of NoV VLPs (5, 75, and 150 ng per well) for 60 min, and NoV VLPs were analyzed by immunoblotting as above (B).

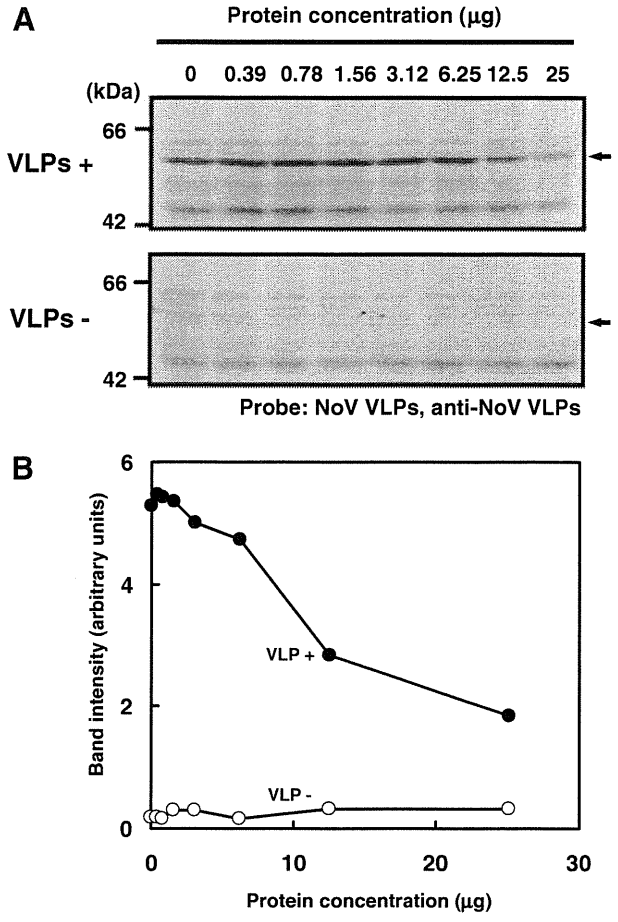

Fig. 4. Suppression of NoV VLP Binding to Caco-2 Cells by Pasteurized Bovine Colostrum.

NoV VLPs (50 ng) and a buffer control without the VLPs were pre-incubated for 15 h at 4 °C with various amounts (0.39–25 μg) of pasteurized bovine colostrum (P-Col), and then incubated with Caco-2 cells for 1 h at 4 °C, followed by immunoblotting analysis for NoV VLPs, as described in the legend to Fig. 3A. The migration position of NoV VP1 is indicated by arrows. The VP1 band intensities were digitized and semi-quantified by densitometric analysis (B). Closed and open circles represent NoV VLPs and the buffer control respectively.

infection indicated that NoV infected and replicated in the epithelial cells of the small intestine.[23] NoV infection at the distal small intestine and colon remains to be investigated. Caco-2 is a cell line established from human colon cancer cells.[10] Nevertheless, Caco-2 cells in confluent culture express several hydrolytic enzymes and nutrient transporters, typical markers of absorptive epithelial cells of the small intestine.[9] Therefore, the observation, in the present and previous studies,[3,7] that NoV VLPs bound to Caco-2 cells, especially differentiated ones, is reasonable. A recent reverse genetic study of human NoV indicated that native NoV could be produced in Caco-2 cells into which NoV genomic RNA had been transfected.[24] Thus it is likely that the NoV-binding assay system established in the present study at least in part reflects or mimics the initial step of *in vivo* NoV infection in the human intestine. This does not necessarily rule out the possibility of NoV infection in human colon epithelia.

Caco-2 cells might consist of heterogeneous cell populations, because they have not necessarily been cloned. The observation that only a small population of colonized Caco-2 cells was positive to NoV VLP binding (Fig. 2) might be explained by this authentic heterogeneity of Caco-2 cells. The frequency of the VLP-binding positive cells in cultured Caco-2 cells increased when the cells were cultured for longer periods (10 d), but the positive cells were still only a minor population (Murakami and Matsuda, unpublished results). NoV VLPs might bind preferentially to differentiated cells in a certain population of Caco-2 cells. In fact, differentiated Caco-2 cells have been reported to be 2–3 times more active in binding with radio-labeled NoV VLPs than undifferentiated cells.[3] From a practical viewpoint, however, the preparation of well-differentiated Caco-2 cells is time consuming and costly. The results of the present study indicate that Caco-2 cells incubated for 3 d were usable in VLP-binding assay based on sensitive immunodetection systems. Thus the VLP-binding assay using undifferentiated Caco-2 cells, *e.g.*, cultured for only 3 d, should have an advantage in high throughput screening of anti-virus factors in food.

NoV VLP-binding to some restricted cells in an all-or-none manner in addition to no binding of SaV VLPs (Fig. 2) indicates that the binding of NoV Ueno-7k VLPs to Caco-2 cells is specific and significant (physiologically or pathologically relevant). Furthermore, almost no binding of NoV VLPs to COS7 cells

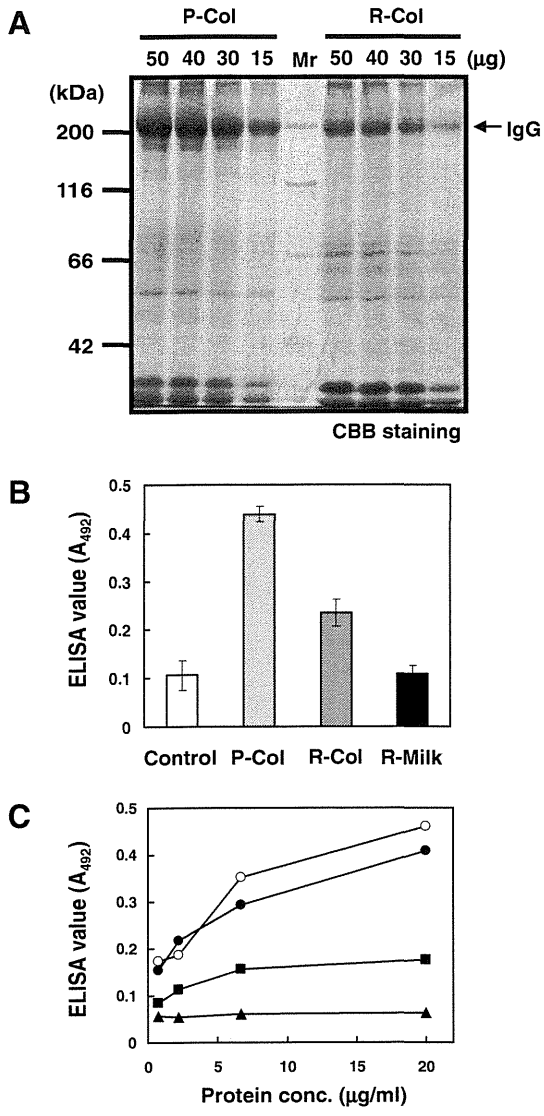

Fig. 5. Bovine Colostrum IgG with Reactivity to NoV- and SaV-VLPs.

Proteins in pasteurized and raw colostrums (P-Col and R-Col respectively) were analyzed comparatively by SDS–PAGE (10% acrylamide gel under non-reducing conditions) (A). ELISA plates were coated with NoV VLPs (0.1 μg/ml) and incubated with 10 μg of protein/ml of P-Col, R-Col, raw milk (R-Milk), and egg albumin as a control. Bovine IgGs bound to the coated VLPs were detected with POD-conjugated anti-bovine IgG (B). ELISA plates were coated with 0.1 μg/ml of NoV VLPs (solid circles and solid triangles), SaV VLPs (open circles), and gelatin (solid squares) as a control and incubated with 10 μg of protein/ml of P-Col. Bovine IgGs bound to the coated VLPs were detected with POD-conjugated anti-bovine IgG. A control assay using POD-conjugated anti-rabbit IgG was also done to test the non-specific binding of the secondary antibody (solid triangles) (C).

(Fig. 3A) suggests that NoV VLP-binding is specific to human intestinal cells. VLP-binding was detected even when only a trace amount of VLPs (5–150 ng) was incubated with Caco-2 cells (Fig. 3B). Based on these results, the binding affinity or avidity of NoV VLPs to Caco-2 cells might not be low. On the other hand, the VP1 band intensity increased almost linearly through an incubation period of 180 min, suggesting that the rate of VLP-binding is low, probably due to the low dispersion rate of VLPs much larger in size than single protein molecules. In the present study, the amounts of VLPs added or bound to the Caco-2 cells were at 10–100 nanogram levels, smaller than previously reported ones (1–10 micrograms), indicating that immunoblotting detection of VLPs using ECL systems has detection-sensitivity higher than the scintillation counting method using VLPs metabolically labeled with ^{35}S-methionine.[3]

Because maternal IgG is not transmitted to the embryo through the placenta in ruminant species of mammals, bovine colostrums contain a large amount of IgG,[13] which is important or critical for newborn calves to gain immunity against environmental pathogens until the development of their own immune systems. The pooled colostrums from healthy and non-immunized cows contained IgG with reactivity to human NoV VLPs, suggesting that cows' colostrums contain naturally occurring antibodies with a large repertory of antigen specificity, including human pathogens. Furthermore, colostrums are known to be rich also in antimicrobial components other than immunoglobulins, including lactoferrin, lactoperoxidase, and lysozyme.[25] Therefore, in addition to colostral IgG, unidentified anti-NoV factors might be present in the colostrums. Hence, colostrums have been expected to contain various immunological and non-immunological defensive factors against enteric pathogens in animals, including humans, but the practical application of bovine colostrums to food as ingredients has been restricted by a Japanese regulatory issue, where bovine colostrums from day 1 to day 5 lactating cows may not be used in food, and moreover milk has to be pasteurized for the market. In the present study, bovine colostrums for P-Col were collected from lactating cows 6–7 d after parturition and heated for pasteurization under mild conditions to prevent or reduce the inactivation of antiviral factors, including antibodies and some other proteins, in the colostrums. In fact, anti-NoV VLPs IgG as well as anti-SaV VLPs IgG was detected in P-Col. Hence, the regulatory and food-safety issues would be resolved at least technically. Bovine colostrums collected at 6 d after parturition or later might be usable in food and food supplements, in which an anti-NoV effect is expected.

Another issue to be discussed is whether such active IgGs escape degradation by digestive enzymes and reach the intestine, where NoV infects the enterocytes. Secretory IgA in human milk and saliva is known to be stabilized by association with a secretory component, and to resistant against digestive enzymes.[12,26] In ruminant animals, including cows, secretory antibodies in colostrums are IgG class,[27] though the secretion mechanisms across the mammary gland epithelium and any structural changes or modifications during secretion remain to be investigated. Some food proteins have been reported to remain intact, at least at immunologically detectable levels, in the lumen of the mouse small intestine.[21,28] It would be of interest to investigate the digestibility or resistance of bovine colostrum IgG *in vitro* and *in vivo* using animal models.

In conclusion, *in vitro* binding-assay using NoV VLPs with Caco-2 cells can be a useful tool in primary screening for anti-NoV in food and natural products, and bovine colostrums have some potential as an infection-protective factor against enteroviruses, including NoV and SaV.

Acknowledgments

This work was supported in part by grant-in-aids for Scientific Research (14360073 and 17658063) from the Ministry of Education, Culture, Sports, Science, and Technology of Japan.

References

1) Griffin MR, Surowiec JJ, McCloskey DI, Capuano B, Pierzynski B, Quinn M, Wojnarski R, Parkin WE, Greenberg H, and Gary GW, *Am. J. Epidemiol.*, **115**, 178–184 (1982).
2) Duizer E, Schwab KJ, Neill FH, Atmar RL, Koopmans MP, and Estes MK, *J. Gen. Virol.*, **85**, 79–87 (2004).
3) White LJ, Ball JM, Hardy ME, Tanaka TN, Kitamoto N, and Estes MK, *J. Virol.*, **70**, 6589–6597 (1996).
4) Jiang X, Wang M, Graham DY, and Estes MK, *J. Virol.*, **66**, 6527–6532 (1992).
5) Green KY, Lew JF, Jiang X, Kapikian AZ, and Estes MK, *J. Clin. Microbiol.*, **31**, 2185–2191 (1993).
6) Huang P, Farkas T, Marionneau S, Zhong W, Ruvoen-Clouet N, Morrow AL, Altaye M, Pickering LK, Newburg DS, LePendu J, and Jiang X, *J. Infect. Dis.*, **188**, 19–31 (2003).
7) Tamura M, Natori K, Kobayashi M, Miyamura T, and Takeda N, *J. Virol.*, **78**, 3817–3826 (2004).
8) Tamura M, Natori K, Kobayashi M, Miyamura T, and Takeda N, *J. Virol.*, **74**, 11589–11597 (2000).
9) Meunier V, Bourrie M, Berger Y, and Fabre G, *Cell Biol. Toxicol.*, **11**, 187–194 (1995).
10) Fogh J, Fogh JM, and Orfeo T, *J. Natl. Cancer Inst.*, **59**, 221–226 (1977).
11) Newburg DS and Walker WA, *Pediatr. Res.*, **61**, 2–8 (2007).
12) Stelwagen K, Carpenter E, Haigh B, Hodgkinson A, and Wheeler TT, *J. Anim. Sci.*, **87**, 3–9 (2009).
13) Barrington GM and Parish SM, *Vet. Clin. North Am. Food Anim. Pract.*, **17**, 463–476 (2001).
14) Newburg DS, *J. Nutr.*, **135**, 1308–1312 (2005).
15) Hansman GS, Natori K, Shirato-Horikoshi H, Ogawa S, Oka T, Katayama K, Tanaka T, Miyoshi T, Sakae K, Kobayashi S, Shinohara M, Uchida K, Sakurai N, Shinozaki K, Okada M, Seto Y, Kamata K, Nagata N, Tanaka K, Miyamura T, and Takeda N, *J. Gen. Virol.*, **87**, 909–919 (2006).
16) Hansman GS, Natori K, Oka T, Ogawa S, Tanaka K, Nagata N, Ushijima H, Takeda N, and Katayama K, *Arch. Virol.*, **150**, 21–36 (2005).
17) Laemmli UK, *Nature*, **227**, 680–685 (1970).
18) Shirato-Horikoshi H, Ogawa S, Wakita T, Takeda N, and Hansman GS, *Arch. Virol.*, **152**, 457–461 (2007).
19) Nakatani H, Aoki N, Nakagawa Y, Jin-No S, Aoyama K, Oshima K, Ohira S, Sato C, Nadano D, and Matsuda T, *Biochem. J.*, **395**, 21–30 (2006).
20) Okumura H, Kohno Y, Iwata Y, Mori H, Aoki N, Sato C, Kitajima K, Nadano D, and Matsuda T, *Biochem. J.*, **384**, 191–199 (2004).
21) Matsubara T, Aoki N, Honjoh T, Mizumachi K, Kurisaki J, Okajima T, Nadano D, and Matsuda T, *Biosci. Biotechnol. Biochem.*, **72**, 2555–2565 (2008).
22) Venkataram Prasad BV, Hardy ME, and Estes MK, *J. Infect. Dis.*, **181** (Suppl 2), S317–S321 (2000).
23) Troeger H, Loddenkemper C, Schneider T, Schreier E, Epple HJ, Zeitz M, Fromm M, and Schulzke JD, *Gut*, **58**, 1070–1077 (2009).
24) Guix S, Asanaka M, Katayama K, Crawford SE, Neill FH, Atmar RL, and Estes MK, *J. Virol.*, **81**, 12238–12248 (2007).
25) Wheeler TT, Hodgkinson AJ, Prosser CG, and Davis SR, *J. Mammary Gland Biol. Neoplasia*, **12**, 237–247 (2007).
26) Woof JM and Kerr MA, *J. Pathol.*, **208**, 270–282 (2006).
27) Stephan W, Dichtelmuller H, and Lissner R, *J. Clin. Chem. Clin. Biochem.*, **28**, 19–23 (1990).
28) Yamada C, Yamashita Y, Seki R, Izumi H, Matsuda T, and Kato Y, *Biosci. Biotechnol. Biochem.*, **70**, 1890–1897 (2006).

THE JOURNAL OF BIOLOGICAL CHEMISTRY VOL. 285, NO. 43, pp. 33175–33183, October 22, 2010
Printed in the U.S.A.

Structure of Hepatitis E Virion-sized Particle Reveals an RNA-dependent Viral Assembly Pathway*[S]

Received for publication, February 5, 2010, and in revised form, August 2, 2010 Published, JBC Papers in Press, August 18, 2010, DOI 10.1074/jbc.M110.106336

Li Xing[‡§1], Tian-Cheng Li[¶1], Naoyuki Mayazaki[‡§], Martha N. Simon[‖], Joseph S. Wall[‖], Mary Moore[‡], Che-Yen Wang[‡], Naokazu Takeda[¶], Takaji Wakita[¶], Tatsuo Miyamura[¶], and R. Holland Cheng[‡2]

From the [‡]Department of Molecular and Cellular Biology, University of California, Davis, California 95616, the [§]Structural Virology Section, Karolinska Institute, Huddinge University Hospital, SE-14186 Stockholm, Sweden, the [¶]Department of Virology II, National Institute of Infectious Diseases, Tokyo 208-0011, Japan, and the [‖]Biology Department, Brookhaven National Laboratory, Upton, New York 11973-5000

Hepatitis E virus (HEV) induces acute hepatitis in humans with a high fatality rate in pregnant women. There is a need for anti-HEV research to understand the assembly process of HEV native capsid. Here, we produced a large virion-sized and a small *T=1* capsid by expressing the HEV capsid protein in insect cells with and without the N-terminal 111 residues, respectively, for comparative structural analysis. The virion-sized capsid demonstrates a *T=3* icosahedral lattice and contains RNA fragment in contrast to the RNA-free *T=1* capsid. However, both capsids shared common decameric organization. The *in vitro* assembly further demonstrated that HEV capsid protein had the intrinsic ability to form decameric intermediate. Our data suggest that RNA binding is the extrinsic factor essential for the assembly of HEV native capsids.

Hepatitis E virus (HEV),[3] the causative agent of acute hepatitis in humans, is primarily transmitted through contaminated water and generally results in epidemic outbreaks in many developing countries. Sporadic cases have also been reported between outbreaks in HEV-endemic regions as well as in non-endemic areas, and these cases are transmitted through zoonotic route. The overall mortality rates of HEV during outbreaks range from 1 to 15% in general, and the highest mortality occurs in pregnant women, with fatality rates of up to 30% (1).

* This work was supported, in whole or in part, by a grant from the National Institutes of Health Roadmap Project on Nanomedicine (to R. H. C.). This work was also supported by grants from the U. S. Department of Agriculture Hatch Fund, STINT Foundation, and Strategic Research Foundation (to R. H. C.). This study was also partly funded by a grant from the Swedish Research Council (to L. X.) and grants for Research on Emerging and Re-emerging Infectious Diseases, Research on Hepatitis, and Research on Food Safety from the Ministry of Health, Labor, and Welfare, Japan (to T.- C. L.).

The atomic coordinates and structure factors (codes 2ZZQ and 3IYO) have been deposited in the Protein Data Bank, Research Collaboratory for Structural Bioinformatics, Rutgers University, New Brunswick, NJ (http://www.rcsb.org/).

The EM data reported in this paper have been submitted to the Electron Microscopy Data Bank (Electron Microscopy Data Bank) with accession number EMD-5173.

[S] The on-line version of this article (available at http://www.jbc.org) contains supplemental Figs. 1–4 and supplemental Table 1.

[1] Both authors contributed equally to this work.

[2] To whom correspondence should be addressed. Dept. of Molecular and Cellular Biology, University of California, Davis CA 95616. Tel.: 530-752-2693; Fax: 530-752-5659; E-mail: rhch@ucdavis.edu.

[3] The abbreviations used are: HEV, hepatitis E virus; VLP, virus-like particle; TEM, transmission electron microscopy; STEM, scanning TEM; TMV, tobacco mosaic virus; DIG, digoxigenin.

HEV consists of a non-enveloped icosahedral capsid and a single-stranded, positive-strand RNA genome of ~7.2 kb that encodes three open reading frames (ORFs) (2). The capsid protein, encoded by the ORF2, is composed of 660 amino acids and responsible for most capsid-related functions, such as virion assembly, host interaction, and immunogenicity. Like other hepatitis viruses, HEV is unable to propagate in currently available cell culture systems, and the research of HEV relies largely on the recombinant HEV capsid proteins (3–6). Virus-like particle (VLP) was obtained when the truncated HEV capsid protein was expressed in insect Tn5 cells with deletion of 52 residues from the C terminus and 111 residues from the N terminus (PORF2) (7). Our previous structural analysis of this HEV-VLP by cryo-electron microscopy (cryo-EM) provided a basic understanding of the quaternary arrangement of PORF2, where the reconstructed VLP displayed a *T=1* icosahedral particle composed of 60 copies of PORF2 (8). The essential element of PORF2 protein for *T=1* VLP assembly includes amino acids 125–600 (9). Recently, the structural information was further refined by the crystal structures of genotype-3 *T=1* VLP (10) and genotype-4 *T=1* VLP (11), which revealed the tertiary structure of PORF2 to the level of amino acids. However, the *T=1* VLPs used in these experiments were much smaller than that of the native virion, which has a diameter of 320–340 Å, as determined by immuno-EM (12). There is still a need to investigate the assembly pathway of HEV capsid.

HEV virion is hypothesized to be made of 180 copies of the capsid protein (8, 11). To test this hypothesis, we screened for HEV genotype expression and successfully produced a virion-sized VLP from the HEV genotype-3 ORF2 protein after deleting 52 residues from the C terminus. This VLP allowed us to investigate the molecular interactions that govern HEV virion assembly.

EXPERIMENTAL PROCEDURES

Production of HEV-VLPs and in Vitro Disassembly and Reassembly—HEV-VLPs were produced and purified according to the protocol described previously (7, 13). Briefly, the recombinant baculovirus Ac(G3n13ORF2), which harbored the genome of the N-terminal 13 amino-acid-deleted genotype-3 HEV ORF2, was infected into Tn5 cells with recombinant baculovirus at a multiplicity of infection of 10. The recombinant baculovirus-infected Tn5 cells were harvested at 7 days after infection. The medium and cells were separated by centrifuga-

tion at 3,000 rpm for 15 min at 4 °C. The cells were treated with a denaturation buffer containing 50 mM sodium borate, 150 mM NaCl, 1% Nonidet P-40, 0.5% sodium deoxycholate, and 5% 2-mercaptoethanol and gently rocked at room temperature for 2 h. The lysate was diluted with EX-CELL 405, and centrifuged at 32,000 rpm for 3 h in a Beckman SW32Ti rotor, and the pellet was resuspended in EX-CELL 405. The VLP was purified by multiple ultracentrifugations followed by separation on a CsCl density gradient. The final pellet was resuspended in 10 mM potassium MES buffer, pH 6.2. A homemade dialysis device was used in the disassembly and reassembly experiments because it allowed dialysis with a small amount of sample (20–40 μl). Purified VLP was disrupted by dialysis against buffer containing EDTA (10 mM) and DTT (20 mM) at different pHs. After VLP dissociation, 150 mM NaCl in Tris-HCl buffer (pH 7.5) was added, and sample was examined under the electron microscope after a 1-h incubation in the presence of the divalent ion Ca^{2+} (20 mM).

Scanning Transmission Electron Microscopy Analysis of HEV-VLPs—Scanning TEM (STEM) was performed at the Brookhaven National Laboratory STEM facility, with tobacco mosaic virus (TMV) as an internal control. The mixture of VLP and TMV was quickly frozen in liquid nitrogen and then maintained at −150 °C during data collection to eliminate contamination and reduce mass loss. The specimen was scanned by a 40-keV electron beam of 0.25 nm in size, and images were collected with a preamp gain of 10 for both large and small angle detectors (14). The image was recorded with a pixel size of 10 Å and was analyzed with the PCMass29 program. After normalizing the background, the mass of the VLPs was selected with the murine sarcoma virus (MSV) shell model provided by the program. Mass measurements for TMV and HEV-VLPs were always performed from the same image. The HEV-VLP mass was measured in MDa (mass per particle), and the TMV mass was measured in KDa/Å (mass per unit length) (15).

Cryo-electron Microscopic Structure Determination of HEV T=3 VLP—The collection of cryo-EM data for image reconstruction was performed on a JEOL JEM-2100F TEM operating at 200 kV according to the procedure described in detail previously (8). Briefly, a 3-μl solution containing VLP or reassembled ORF2 complex was placed on holey carbon film-coated copper grids and then quickly plunged into liquid ethane after the removal of excess solution. The VLPs were embedded into a thin layer of vitrified ice and transferred into the EM using a Gatan 626 cryo-transferring system. The specimen was observed under 50,000× magnification, and the area of interest was recorded on a TVIPS CCD camera (TemCam-F415). The micrographs were recorded with a pixel size of 2.0 Å at a specimen space and defocus level of 0.7–3.5 Å (supplemental Fig. 1*A*). Digital images with no stigmatism or drift were selected for later image processing. Images of individual HEV *T=3* VLPs were then boxed out and processed with an established software package for icosahedral particles (16, 17). In total, 7,720 individual images were included in the process, and their defocus levels were distributed mainly within 1.0–2.5 Å.

To correct contrast transfer function effect, we applied phase flipping on each image with an in-house program. The density maps were initially reconstructed by combining 1,812 individual images to an effective resolution of 14 Å. Next, amplitude correction was applied during map reconstruction while new data were added. The final density map was reconstructed by combining images of 4,348 individual particles, and the final resolution was assessed as 10.6 Å by Fourier shell correlation with a cutoff of 0.5 (supplemental Fig. 1*B*).

Docking of the *T=1* crystal structure into the *T=3* cryo-EM density map was first done manually with the program O (18) and then refined with the Situs software package (19). The PORF2 monomer was treated as a rigid body during the initial fitting and refinement processes.

X-ray Crystallographic Structure Determination of T=1 HEV-VLP—Crystallization of the VLPs was performed according to a previously described method (20). Crystals were directly flash-frozen in liquid nitrogen, and x-ray diffraction experiments were performed. All x-ray experiments of the HEV-VLP crystals were performed at SPring-8 in Hyogo, Japan. Particle orientation in the unit cell was determined with a self-rotation function (21), and the particle position was determined by a translation search with the cryo-EM structure as the model. The asymmetric crystal unit contains one particle; as a result, 60-fold non-crystallographic symmetry averaging was enforced. The cryo-EM structure (8) was used to obtain the initial phases of Data I (supplemental Table 1) and generated the envelope (mask) used for non-crystallographic symmetry averaging. The phases were refined by real space electron density averaging with icosahedral symmetry elements and solvent flattening. The resolution was gradually extended to 8.3 Å (*R*-factor = 0.21, correlation coefficient = 0.92). This structure was used for the phasing of Data II (supplemental Table 1), and the phases were refined and extended to a 3.8 Å resolution (the overall *R*-factor and correlation coefficient were 0.18 and 0.97, respectively). The electron density map revealed a clear main chain structure. Thus, we built an atomic model into this electron density map using the program O (18) without difficulty.

Sixty icosahedrally related S-subunits were treated as identical, and strict non-crystallographic symmetry constraints were applied during refinement. The data with the resolution range of 20–3.8 Å were included in the refinement (supplemental Table 1 and supplemental Fig. 2) using the CNS program (22). The subunit position and orientation were again clarified by rigid body refinement (*R*-factor of 0.391 (R_{free} = 0.395)). After the first cycle of simulated annealing refinement, positional and *B*-factor refinement followed, and the model was enhanced to an *R*-factor of 0.261 (R_{free} = 0.264). Further positional and *B*-factor refinement, followed by manual revision of the model, resulted in an *R*-factor of 0.242 (R_{free} = 0.245) with reasonable stereochemistry (root mean square deviations in bond lengths and bond angles were 0.010 Å and 1.68°, respectively). Because of the high non-crystallographic symmetry, the *R*-factor and R_{free} factor were almost identical. After refinement, the stereochemistry of the structure was checked with Procheck (23). 98.1% of the non-glycine residues were within the most favored and the additional allowed regions of the Ramachandran plot, and none of the residues were in the additional regions. Atomic structure representations were generated using MolScript (24) and Raster3D (25).

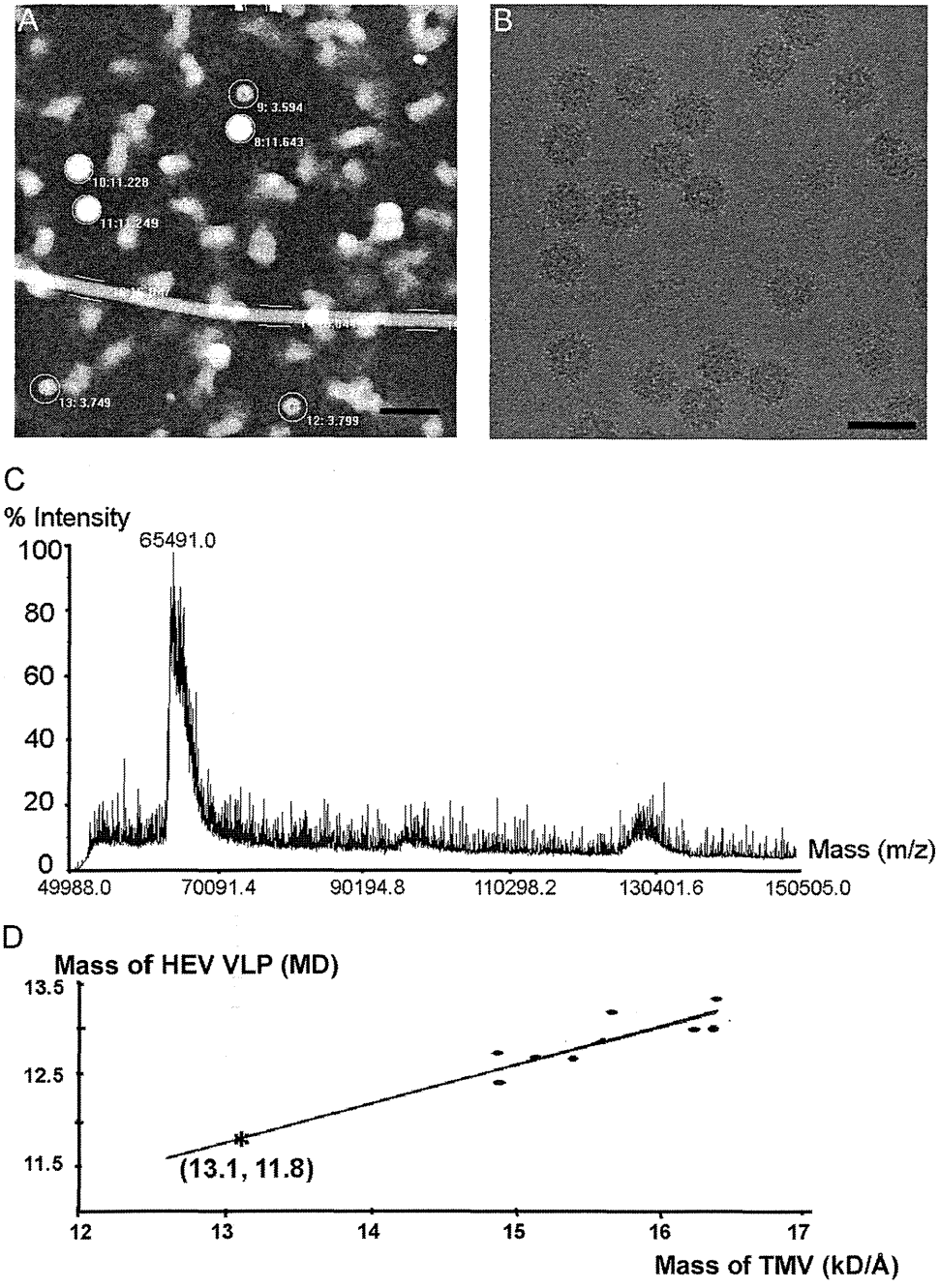

FIGURE 1. **The large HEV-VLP is composed of 180 copies of ORF2 protein.** *A*, STEM micrograph of HEV-VLPs. Both large and small *T=1* HEV-VLPs are projected as spherical images, and their corresponding particle mass was calculated. The long straight rod is TMV, which was added as an internal mass standard. (*Bar* = 1,000 Å.) *B*, the large HEV-VLP appeared as an intact particle decorated with a dot-like pattern on the surface on cryo-EM of the large HEV-VLP. (*Bar* = 500 Å.) *C*, mass spectrum of the large HEV-VLP showing that the molecular mass of the ORF2 protein is 65.5 kDa. *D*, plot showing the observed mass/length of TMV against the observed mass of the large HEV-VLP from different image conditions. For a known TMV mass/length of 13.1 kDa/Å, the mass of the large HEV-VLP was calculated as 11.8 MDa (*asterisk*). *MD*, megadalton.

Nucleic Acid Extraction and Characterization—100 μg of purified large and small VLPs were treated with DNase I (final concentration; 0.01 mg/ml) (Sigma) and RNase A (final concentration; 0.5 μg/ml) at 37 °C for 1 h and then followed by centrifugation at 50,000 rpm for 2 h at 4 °C in a Beckman TLA55Ti rotor. After removal of the supernatant, the pellets were resuspended in 200 μl of PBS minus buffer. The nucleic acids were extracted with RNAzol-LS reagent (Tel-test, Inc., Friendswood, TX) and analyzed on 1% agarose gels.

For detection of HEV RNA in VLPs, the extracted RNAs from VLPs were mixed with sample buffer (final concentration: 2% formaldehyde, 50% formamide in MOPS buffer containing 20 mM MOPS, 5 mM sodium acetate, and 1 mM EDTA (pH 7.0), Sigma-Aldrich, Tokyo, Japan). The solution was denatured at 65 °C for 10 min and cooled immediately in ice-cold water and then mixed with 6× loading buffer (80% formamide, 0.25% bromphenol blue, 0.25% xylene cyanol, 6 mM EDTA, Sigma-Aldrich). After separation on the formaldehyde-denatured agarose gel (18% formaldehyde, 1% agarose, Sigma-Aldrich) in 1× MOPS buffer, the gel was washed twice for 15 min with 20× SSC (3 M NaCl, 0.3 M trisodium citrate dehydrate (pH 7.0), Roche Applied Science, Tokyo, Japan) and transferred onto a Hybond N^+ membrane filter (GE Healthcare, Tokyo, Japan) by the capillary method. RNAs were fixed on the membrane by irradiation with UV light (Stratalinker UV crosslinker, Stratagene, Tokyo, Japan) and dried in the air. RNAs on the membrane were hybridized with DIG-labeled probe. DIG-labeled RNAs were detected by using a DIG Northern starter kit (Roche Applied Science) according to the manufacturer's protocol and visualized by the LAS-3000 imaging analyzer, Fujifilm, Tokyo, Japan). The purified template DNA for the probe RNA was prepared by digesting the plasmid carrying 584-base cDNA of HEV ORF2 (5,903–6,486 nucleotides) under the T7 promoter with BamHI. The probe RNA was prepared using the DIG Northern starter kit according to the manufacturer's manual (incorporation of DIG-UTP during RNA transcription). The norovirus-like particles that were produced by the recombinant baculovirus were used as a control, and the same procedure was used with the HEV-VLPs.

RESULTS

STEM—The virion-sized HEV-VLP was recovered when the genotype-3 ORF2 sequence was expressed in insect cells. This VLP projected as a spherical image with a diameter of ~40 nm, larger than the *T=1* VLP (27 nm in diameter) (Fig. 1*A*). In

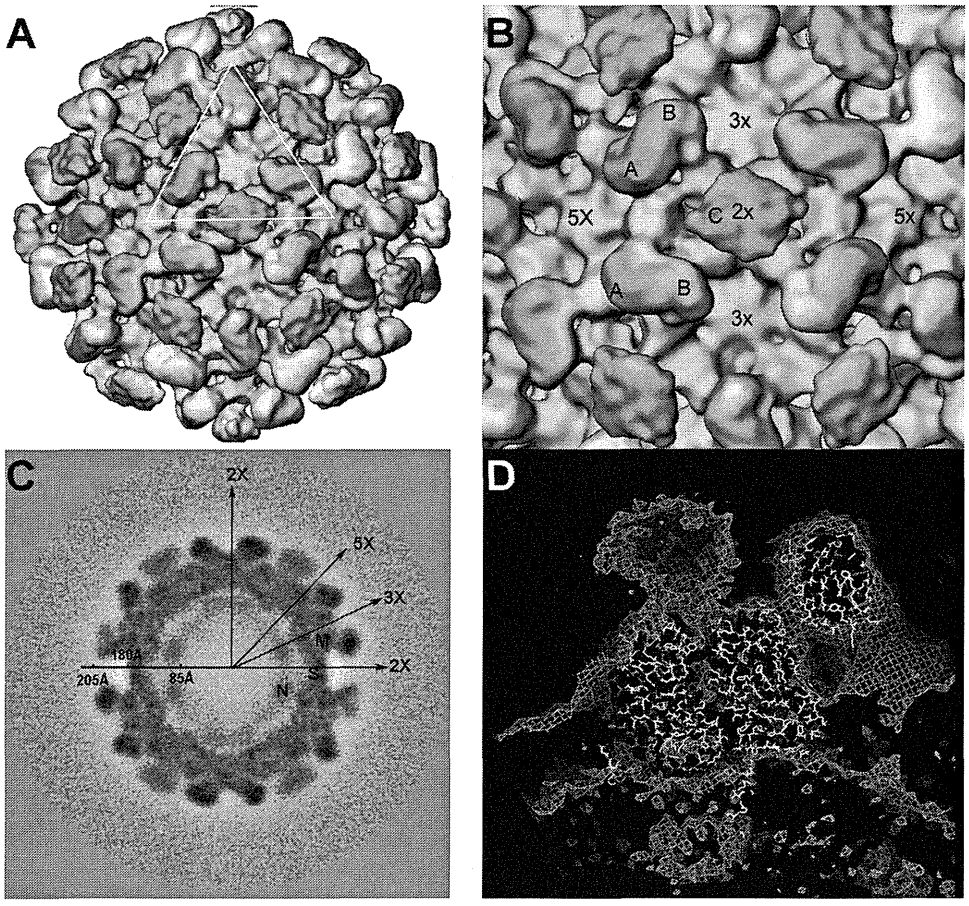

FIGURE 2. **Three-dimensional structure of HEV *T=3* VLP.** *A*, overall structure of the large HEV-VLP reveals the *T=3* icosahedral lattice of the ORF2 proteins. One icosahedral facet is defined as the *triangular area* within the three adjacent five-fold axes. *B*, there are two unique dimeric ORF2 spikes on the HEV *T=3* VLP surface. The A-B dimer is located around the five-fold axis, and the C-C dimer is located at the two-fold axis. *C*, HEV *T=3* VLP has a radius of 205 Å and contains a low density cavity with a radius of 85 Å in the particle center. The distribution of the cryo-EM density revealed four ORF2 domains, P, M, S, and N, at 50 Å from the equatorial section. *D*, the crystal structure of the HEV subunit from *T=1* VLP docks well with the cryo-EM density in the shell region of HEV *T=3* VLP, with the N-terminal loop pointing toward the center.

cryo-electron micrographs, the images of HEV-VLP are decorated with spike-like features and are homogeneous in contrast (Fig. 1*B*).

To determine the composition of the large HEV-VLP, we performed mass measurements by using STEM, a technique that measures the amount of electrons scattered from the objects, such as VLPs, on an EM grid. A mixture of purified large and small HEV-VLPs was freeze-dried onto EM grids for STEM mass measurement. TMV with a known mass-to-length ratio was used as an internal standard. The HEV-VLPs appeared as spherical projections with white contrast on the dark field STEM images (Fig. 1*A*). White cloud-like objects were present in the background, which might be the VLPs broken during sample preservation. The mean mass of large VLP and TMV in the images was measured to generate a plot of the mean TMV mass per unit length *versus* mean VLP mass per particle (Fig. 1*A*). A first-order fit was calculated, and the mass of the large HEV-VLP was determined to be 11.8 MDa (Fig. 1*D*). The mass of the genotype-3 ORF2 protein, which was recovered from the large VLP, was measured as 65.5 KDa by mass spectrometry (Fig. 1*C*). Therefore, the large HEV-VLP contains 180 copies of ORF2 proteins, suggesting that the large HEV-VLP is a *T=3* icosahedral particle (*T=3* VLP). We further performed element analysis with x-ray photoelectron spectroscopy. X-ray photoelectron spectroscopy, also known as electron spectroscopy for chemical analysis, determines the chemical composition of the sample with a depth of 50–70 nm. Phosphorus element, as a characteristic element of nucleic acid, was detected from the G3-VLP that was applied to the carbon-coated copper grid (supplemental Fig. 1*C*). Although the signal of phosphorus element is weak when compared with that of carbon, the phosphorus peak is not detectable in the control grid without VLP materials. This result suggests the co-existence of nucleic acid within the large G3-VLPs.

Three-dimensional Reconstruction of the HEV Virion-sized Particle—The cryo-EM structure of the large HEV-VLP revealed 90 protruding spikes on a complete icosahedral shell (Fig. 2*A*), which is consistent with the *T=3* icosahedral symmetry and the results of the STEM mass measurements. The VLP had an overall diameter of 410 Å and a central cavity of 170 Å in radius as measured from the three-dimensional density map (Fig. 2*C*). The single-layer capsid contained 180 copies of the ORF2 protein, which were grouped into three unique monomers according to their geometric environments. Although monomers A and B formed dimeric spikes (A-B dimers) around each of the five-fold axes, two two-fold related C monomers formed a spike (C-C dimer) at each of the icosahedral two-fold axes (Fig. 2*B*). The surface lattices of ORF2 proteins in HEV *T=3* VLP were similar to the capsid arrangement of caliciviruses. When compared with the A-B dimer, the morphology of the HEV C-C dimer was less well defined, perhaps due to flexibility in the angle of the protruding domain toward the icosahedral shell.

The density map of the *T=3* VLP displayed four discrete domains, designated from the outside inward as P, M, S, and N, on a section 52 Å from the equatorial plane (Fig. 2*C*). The density profile of the P, M, and S domains displayed less variation from that observed in *T=1* HEV-VLP, and the docking of the crystal structure of the *T=1* PORF2 protein to the density map of *T=3* HEV-VLP showed a very good agreement between the two structures (Fig. 2*D*). The docking positioned N-terminal tail of the PORF2 protein at the capsid inner surface aligned well with the density linker in *T=3* VLP (Fig. 2*D*). The linker density served as a tag to connect the N domain with the icosahedral capsid, indicating the

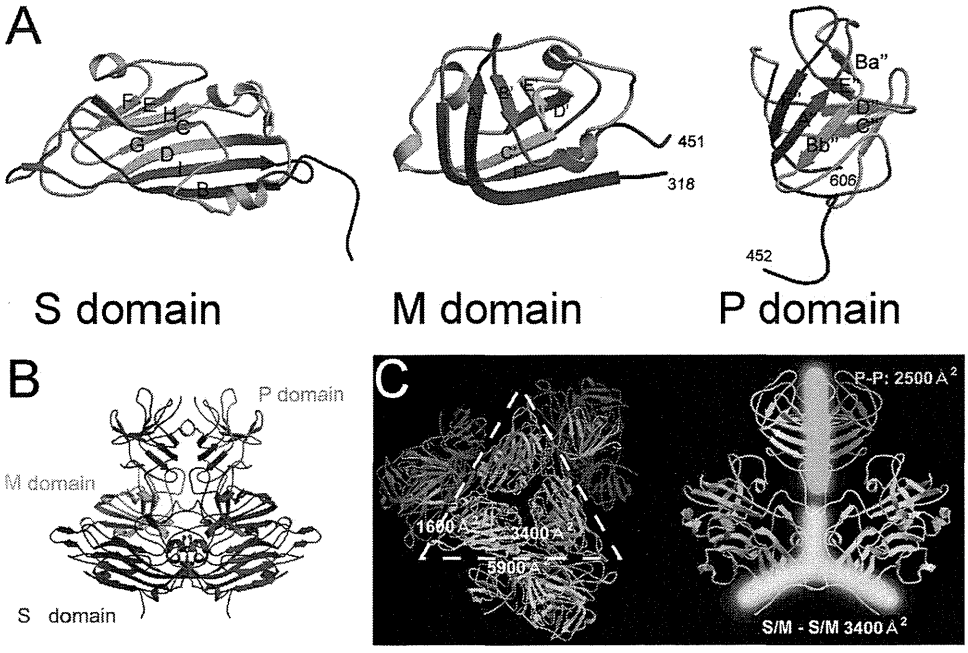

FIGURE 3. **The structure of genotype-1 PORF2 protein.** *A*, ribbon representations of S, M, and P. The structure is covered from *blue* (N terminus of the domain) to *red* (C terminus of the domain). *B*, dimer structure of the capsid protein. One subunit is colored *red*, and the other subunit is colored according to its domain structure (*blue*, S domain; *green*, M domain; *orange*, P domain). *C*, surface areas that buried at the interfaces between two adjacent subunits are overlapped with a PORF2 hexamer (*left*) and at the PORF2 dimeric interface (*right*). One icosahedral facet is defined as the *triangular area* within the three adjacent five-fold axes.

location of the N-terminal 111 amino acids of the ORF2 protein in *T=3* HEV-VLP.

Crystal Structure of the Genotype-1 T=1 HEV-VLP—The crystal structure of the truncated genotype-1 capsid protein (PORF2, containing residues 112–608) can be separated into three domains, S, M, and P, with a less resolved region covering residues 555–560. The S domain formed by residues 118–317 folds into a classical eight-stranded β-barrel with a jelly roll motif (Fig. 3*A*), as observed in many *T=3* viral capsid proteins (26, 27). Uniquely, three additional short α-helixes were observed in the S domain between strands E and F and strands G and H. The capsid shell was mainly stabilized by intersubunit interactions between the S domains. The folded M domain, consisting of residues 318–451, was a twisted antiparallel β-sheet with an α-helix between the B′ and C′ strands (Fig. 3*A*). The P domain, composed of residues 452–606, folded into a β-barrel composed of antiparallel β-sheets, F″A″Bb″ and Ba″E″D″C″ (Fig. 3*A*), and was connected with the M domain through a long proline-rich hinge (PTPSPAPSRP of residues 452–461) (Fig. 3*A*). Although both the M and the P domains existed above the S domain, the protruding spikes in the HEV cryo-EM map contain only the P domain density, which is a clear difference to those caliciviruses (supplemental Fig. 3). The PORF2 dimers have the largest buried surface area between monomers (5,900 Å^2) mainly due to the interface between P domains (Fig. 3*B*). The buried surface area is 3,400 and 1,600 Å^2 for the two adjacent PORF2 subunits around a three-fold axis and a five-fold axis, respectively (Fig. 3*B*). Moreover, the buried surface area of three molecules around a three-fold axis (9,500 Å^2) is much wider than that around a five-fold axis (4,700 Å^2).

Sequence alignment of genotype-1 PORF2 with the sequences of genotype-3 (10) and genotype-4 (11) revealed that the S domain is the most conserved region among HEV genotypes, whereas greater divergence was seen in the N-terminal region (supplemental Fig. 4*A*). Among the solved structures, genotype-3 appeared flexible at the N-terminal end and was 11 amino acids shorter than the others, whereas the structure deviation from genotype-1 PORF2 is very small (total root mean square deviation is 0.62 for the 472 equivalent amino acids) (supplemental Fig. 4*B*). Because amino acids 118–129 play an important role in bridging the N-domain to the S-domain in *T=3* VLP and serve as a docking register, we used the crystal structure of genotype-1 to decipher the *T=3* cryo-EM density map.

Consistent Interdimeric Interactions between T=3 and T=1 HEV-VLPs—To understand the mechanism of ORF2 protein transition between *T=1* and *T=3* assemblies, we docked the *T=1* decamer and hexamer into the *T=3* cryo-EM density map. The decamer of *T=1* VLP consisted of 10 adjacent PORF2 monomers corresponding to five dimers around a five-fold axis, whereas the *T=1* hexamer corresponded to three adjacent dimers around a three-fold axis. Unlike the hexamer, the coordinates of the PORF2 decamer fitted very well with the curvature of the *T=3* density map at the five-fold vertex (Fig. 4*A*) and with the domain separation (Fig. 4*B*). The curvature of *T=3* capsid at the three-fold axis did not agree with the coordinates of the PORF2 hexamer as one of the dimers appeared to be sticking out of the cryo-EM density map (data not shown). Besides, the orientation of the P domain of the C-C dimer relative to its M/S domains was 90° different from that of the A-B dimer (Fig. 5). This suggests that the molecular interactions among A-B dimers in the *T=3* icosahedron are consistent with the dimer-dimer interactions in the *T=1* icosahedral assembly, whereas the interaction between the A-B dimer and C-C dimer is unique to the *T=3* assembly.

In Vitro Reassembly of the ORF2 Protein—To understand the role of ORF2 decamer in *T=3* VLP assembly, we analyzed the self-assembly process of HEV-VLP *in vitro*. A combination of chelating (EDTA) and reducing (DTT) agents was found to disassemble *T=3* VLP in a high alkaline environment (pH 10) without denaturating the ORF2 protein (data not shown). The addition of 20 mM $CaCl_2$ into the disassembly solution led to the association of the ORF2 dimers into star-shaped complexes, and no refolded VLP was found (Fig. 4*C*). When we examined the star-shaped complexes, we found that the distance between two opposite vertices was ~18 nm, close to the diameter of TMV (Fig. 4*D*). This size was consistent with that measured from PORF2 decamers. Thus, the star-shaped complexes resembled not only the appearance but also the size of the ORF2